Cumulant-Based Inverse Filter Criteria for MIMO Blind Deconvolution: Properties, Algorithms, and Application to DS/CDMA Systems in Multipath

Chong-Yung Chi, *Senior Member, IEEE,* and Chii-Horng Chen

***Abstract*—Tugnait and Chi and Chen proposed multi-input multi-output inverse filter criteria (MIMO-IFC) using higher order statistics for blind deconvolution of MIMO linear time-invariant systems. This paper proposes three properties on the performance of the MIMO linear equalizer associated with MIMO-IFC for any signal-to-noise ratio, including P1) perfect phase equalization property, P2) a relation to MIMO minimum mean square error (MIMO-MMSE) equalizer, and P3) a connection with the one obtained by MIMO super-exponential algorithm (MIMO-SEA) that usually converges fast but does not guarantee convergence for finite data. Based on P2), a fast algorithm for computing the theoretically optimum MIMO equalizer is proposed. Moreover, based on P3), a fast MIMO-IFC based algorithm with performance similar to that of the MIMO-SEA and with guaranteed convergence is proposed as well as its application to suppression of multiple access interference and intersymbol interference (ISI) for multiuser asynchronous DS/CDMA systems in multipath. Finally, some simulation results are presented to support the analytic results and the proposed algorithms.**

***Index Terms*—Cumulants, inverse filter criteria, MIMO blind deconvolution.**

I. Introduction

BLIND deconvolution of a multi-input multi-output (MIMO) linear time-invariant (LTI) system, which is denoted $\mathbf{H}[n]$ ($P \times K$ matrix), is a problem of estimating the vector input $\mathbf{u}[n] = (u_1[n], \cdots, u_K[n])^T$ (K inputs) with only a set of non-Gaussian vector output measurements $\mathbf{x}[n] = (x_1[n], \cdots, x_P[n])^T$ (P outputs) as follows: [1]–[4]

$$\mathbf{x}[n] = \sum_{k=-\infty}^{\infty} \mathbf{H}[k]\mathbf{u}[n-k] + \mathbf{w}[n] \tag{1}$$

where $\mathbf{w}[n]$ ($P \times 1$ vector) is additive noise. The MIMO LTI system arises in science and engineering areas where multiple sensors are needed such as time delay estimation, source separation, and sesimic signal processing, etc. In communications, multiple antennas receiving signals and oversampling of received signals can also be modeled as MIMO LTI systems on which a variety of detection and estimation algorithms are based [2]–[4].

Manuscript received September 29, 2000; revised April 3, 2001. This work was supported by the National Science Council, R.O.C., under Grants NSC 88-2218-E-007-019 and NSC 89-2213-E-007-093. Part of this work was presented at the Tenth IEEE Workshop on Statistical Signal and Array Processing, Poconos Manor, PA, August 13-16, 2000. The associate editor coordinating the review of this paper and approving it for publication was Dr. Alex B. Gershman.

The authors are with the Department of Electrical Engineering, National Tsing Hua University, Hsinchu, Taiwan, R.O.C.

Publisher Item Identifier S 1053-587X(01)05177-7.

Higher order statistics (HOS), known as cumulants [5], have been used for blind deconvolution of nonminimum-phase LTI systems with a given set of non-Gaussian measurements. There have been a lot of blind deconvolution algorithms reported in the open literature [6]–[13] for nonminimum-phase single-input single-output (SISO) systems ($P = K = 1$) using HOS. Chi and Wu [6] proposed a family of SISO inverse filter criteria (SISO-IFC) that includes Wiggins's criterion [7], Shalvi and Weinstein's criterion [8], and Tugnait's criteria [9] as special cases. Under the assumptions a1) the signal-to-noise ratio (SNR) is infinity, and a2) the length of equalizer is infinite, it has been shown that SISO-IFC achieve perfect equalization, i.e., the equalizer (inverse filter) output is equivalent to the input signal except for an unknown scale factor and an unknown time delay. Feng and Chi [11], [12] reported some performance analyses of SISO-IFC for finite SNR that are helpful in the interpretation of the deconvolved signals and to realizing the behavior of the designed equalizer. Shalvi and Weinstein [13] proposed an SISO super exponential algorithm (SISO-SEA) for blind deconvolution that converges at a super exponential rate under the assumptions a1) and a2). Recently, it was shown [14] that for finite SNR and equalizer's length, the optimum inverse filter obtained by SISO-IFC and that obtained by SISO-SEA [13] are equivalent if second- and fourth-order cumulants are used; meanwhile, they are also equivalent to that obtained by the well-known constant modulus algorithm (CMA) [15].

Blind deconvolution algorithms for nonminimum-phase MIMO LTI systems using HOS have also been reported [16]–[28] in the past decade. Tugnait [16] proposed MIMO-IFC for blind deconvolution of MIMO systems using second- and third-order cumulants or second- and fourth-order cumulants of inverse filter (equalizer) output. Under assumptions a1) and a2), the optimum inverse filter output turns out to be one of the input signals except for an unknown scale factor and an unknown time delay (i.e., the optimum inverse filter is a perfect equalizer for one of the input signals). All the input signals can be estimated through a multistage successive cancellation (MSC) procedure [16]. Furthermore, based on the MIMO-IFC and the MSC procedure, Tugnait [17] proposed adaptive blind MIMO deconvolution algorithms under assumption a1). Chi and Chen [18] further extended Tugnait's MIMO-IFC using second- and higher order (≥ 3) cumulants of inverse filter output with application to suppression of multiple access interference (MAI) and intersymbol interference (ISI) for multiuser DS/CDMA systems.

Some other inverse filter criteria using second- and fourth-order cumulants of inverse filter output for MIMO blind deconvolution have been reported in [19]–[21] with which the designed equalizer also performs as a perfect equalizer under assumptions a1) and a2). Assuming that the input vector $\mathbf{u}[n]$ satisfies the normalized whitening condition, i.e., $u_i[n]$, $i = 1, \cdots, K$ are white random processes with unit variance and they are mutually uncorrelated, Inouye and Habe [19] proposed a constrained multistage inverse filter criterion. Based on the constrained multistage inverse filter criterion, Inouye and Sato [20] further proposed an unconstrained multistage inverse filter criterion. Inouye [21] also proposed a constrained single stage inverse filter criterion that has been shown to be equivalent to the constrained multistage inverse filter criterion reported in [19].

Yeung and Yau [22] and Inouye and Tanebe [23] also proposed MIMO-SEA for blind deconvolution. Again, under assumptions a1) and a2), the designed equalizer by the MIMO-SEA is also a perfect equalizer (for one of the input signals) with a super-exponential convergence rate, and all the input signals are estimated through the MSC procedure in a nonsequential order. Moreover, the SISO-SEA for fractionally spaced equalization [24], which turns out to be an MIMO-SEA, and the MIMO-CMA [25]–[27] have been reported for blind deconvolution under assumption a1). To our knowledge, the performance of all the above mentioned MIMO blind deconvolution algorithms for finite SNR is unknown so far. Moreover, both the SISO-SEA and MIMO-SEA may diverge for finite SNR and finite data in spite of their fast convergence for infinite SNR and sufficient data.

Ding and Nguyen [28] proposed a performance analysis for a beamformer using kurtosis maximization algorithm (KMA) that is actually a special case of Chi and Chen's MIMO-IFC using second- and fourth-order cumulants. The global convergence property of the KMA together with the optimum beamformer perfectly capturing a single source for infinite SNR has been shown. Moreover, for finite SNR, the optimum beamformer performs as a minimum mean square error (MMSE) beamformer only for the case of single source ($K = 1$) as the kurtosis of noise is equal to zero, whereas the performance of the optimum beamformer for multiple sources ($K \geq 2$) and finite SNR is still unknown.

In this paper, three properties on the performance of cumulant based MIMO-IFC [16]–[18] are proposed. Based on the presented properties, a fast algorithm for computing the theoretically optimum MIMO equalizer, and a fast MIMO-IFC based algorithm with performance similar to that of MIMO-SEA [22], [23] and with guaranteed convergence, are proposed. Moreover, an application of the latter to MAI and ISI suppression for multiuser asynchronous DS/CDMA systems is also presented.

The paper is organized as follows. Section II presents a brief review of MIMO-IFC and MIMO-SEA for blind deconvolution of MIMO systems. Section III presents three properties of the optimum equalizer associated with MIMO-IFC, a fast algorithm (Algorithm 1) for obtaining the true equalizer needed in the simulation stage, and a fast MIMO-IFC based algorithm (Algorithm 2) with guaranteed convergence. Section IV presents the MIMO model for asynchronous DS/CDMA systems followed by blind deconvolution processing using Algorithm 2. Then some simulation results are presented in Section V to support the presented analytic results and the efficacy of Algorithm 2. Finally, we draw some conclusions.

II. Review of MIMO-IFC and MIMO-SEA

Let $\text{cum}\{y_1, y_2, \cdots, y_p\}$ denote the pth-order cumulant of random variables y_1, $y_2, \cdots, y_p$ [5], and let $\mathcal{F}\{\cdot\}$ denote discrete-time Fourier transform operator. For ease of later use, let us define the following notations:

$$\begin{aligned}
\text{cum}\{y:p,\cdots\} &= \text{cum}\{y_1 = y, y_2 = y, \cdots, y_p = y, \cdots\} \\
C_{p,q}\{y\} &= \text{cum}\{y:p, y^*:q\} \\
&\quad (y^* \text{ is complex conjugate of } y) \\
\boldsymbol{v}_j &= (v_j[L_1], v_j[L_1+1], \cdots, v_j[L_2])^T \\
&\quad ((L = L_2 - L_1 + 1) \times 1 \text{ vector}) \\
\boldsymbol{\nu} &= (\boldsymbol{v}_1^T, \boldsymbol{v}_2^T, \cdots, \boldsymbol{v}_P^T)^T \\
\boldsymbol{\varepsilon}_j &= K \times 1 \text{ unit column vector with the} \\
&\quad j\text{th entry equal to unity} \\
\boldsymbol{x}_j[n] &= (x_j[n-L_1], x_j[n-L_1-1] \\
&\quad \cdots, x_j[n-L_2])^T \\
\tilde{\boldsymbol{x}}[n] &= (\boldsymbol{x}_1^T[n], \boldsymbol{x}_2^T[n], \cdots, \boldsymbol{x}_P^T[n])^T \\
\boldsymbol{R}_{i,j} &= E[\boldsymbol{x}_i^*[n]\boldsymbol{x}_j^T[n]] \quad (L \times L \text{ matrix}) \\
\tilde{\boldsymbol{R}} &= \{\boldsymbol{R}_{i,j}\} \quad (P \times P \text{ block matrix}).
\end{aligned}$$

Assume that we are given a set of measurements $\mathbf{x}[n]$, $n = 0, 1, \cdots, N-1$ modeled by (1) with the following assumptions:

- $\mathcal{A}1$) $u_j[n]$ is zero-mean, independent identically distributed (i.i.d.) non-Gaussian with $(p+q)$th-order cumulant $C_{p,q}\{u_j[n]\} \neq 0$ and variance $\sigma_{u_j}^2 = C_{1,1}\{u_j[n]\}$ and statistically independent of $u_k[n]$ for all $k \neq j$.
- $\mathcal{A}2$) The MIMO system $\mathbf{H}[n]$ is exponentially stable.
- $\mathcal{A}3$) The noise $\mathbf{w}[n]$ is zero-mean colored Gaussian with covariance matrix $\mathbf{Q}[k] = E[\mathbf{w}[n]\mathbf{w}^H[n-k]]$ and statistically independent of $\mathbf{u}[n]$.

Let $\mathbf{v}[n] = (v_1[n], v_2[n], \cdots, v_P[n])^T$ denote a linear FIR equalizer of length $L = L_2 - L_1 + 1$ for which $\mathbf{v}[n] \neq \mathbf{0}$ for $n = L_1, L_1+1, \cdots, L_2$. Then, the output $e[n]$ of the FIR equalizer $\mathbf{v}[n]$ can be expressed as

$$\begin{aligned}
e[n] &= \sum_{j=1}^{P} v_j[n] * x_j[n] = \sum_{j=1}^{P} \boldsymbol{v}_j^T \boldsymbol{x}_j[n] \\
&= \boldsymbol{\nu}^T \tilde{\boldsymbol{x}}[n] \qquad (2) \\
&= \sum_{k=1}^{K} s_k[n] * u_k[n] + w[n] \\
&= \sum_{k=-\infty}^{\infty} \mathbf{s}^T[k]\mathbf{u}[n-k] + w[n] \quad \text{[by (1)]} \qquad (3)
\end{aligned}$$

where "$*$" denotes the discrete-time convolution operator

$$\begin{aligned}
\mathbf{s}[n] &= (s_1[n], \cdots, s_K[n])^T \\
&= \mathbf{H}^T[n] * \mathbf{v}[n] = \sum_{l=L_1}^{L_2} \mathbf{H}^T[n-l]\mathbf{v}[l] \qquad (4)
\end{aligned}$$

and

$$w[n] = \sum_{j=1}^{P} v_j[n] * w_j[n]. \tag{5}$$

With the assumptions $\mathcal{A}1$)–$\mathcal{A}3$), it can be easily shown from (2), (3), and (5) that the correlation function $r_{ww}[k]$ of the Gaussian noise $w[n]$ can be expressed as

$$\begin{aligned} r_{ww}[k] &= E[w[n]w^*[n-k]] \\ &= \sum_{n_1=-\infty}^{\infty} \sum_{n_2=-\infty}^{\infty} \mathbf{v}^T[n_1]\mathbf{Q}[k+n_2-n_1]\mathbf{v}^*[n_2] \\ &= \sum_{l=1}^{P} \sum_{i=1}^{P} [\mathbf{Q}[k]]_{il} * v_i[k] * v_l^*[-k] \end{aligned} \tag{6}$$

where $[\mathbf{Q}[k]]_{il}$ is the ith component of the lth column of $\mathbf{Q}[k]$ and that

$$C_{1,1}\{e[n]\} = \sum_{i=1}^{K} \sigma_{u_i}^2 \left(\sum_{n=-\infty}^{\infty} |s_i[n]|^2 \right) + r_{ww}[0] \tag{7}$$

$$C_{p,q}\{e[n]\} = \sum_{i=1}^{K} C_{p,q}\{u_i[n]\} \left(\sum_{n=-\infty}^{\infty} s_i^p[n](s_i^*[n])^q \right) \quad p+q \geq 3 \tag{8}$$

since $C_{p,q}\{w[n]\} = 0$ for all $p+q \geq 3$.

The designed equalizer is usually evaluated by the amount of ISI defined as [10], [22]

$$\mathrm{ISI}(e[n]) = \frac{\left\{ \sum_{k,n} |s_k[n]|^2 \right\} - \max_{k,n}\{|s_k[n]|^2\}}{\max_{k,n}\{|s_k[n]|^2\}}. \tag{9}$$

The smaller the ISI$(e[n])$, the better the performance of the designed equalizer $\mathbf{v}[n]$, whereas it is actually a function of the overall channel $\mathbf{s}[n]$ after equalization. Note that ISI$(e[n]) = 0$ (perfect equalization in the absence of noise) as $\mathbf{s}[n] = \alpha \cdot \boldsymbol{\epsilon}_\ell \cdot \delta[n-\tau]$ (i.e., $s_\ell[n] = \alpha\delta[n-\tau]$ and $s_k[n] = 0$ for $k \neq \ell$), where $\alpha \neq 0$, and τ is an integer.

Chi and Chen [18] find the optimum $\boldsymbol{\nu}$ by maximizing the following MIMO-IFC:

$$J_{p,q}(\boldsymbol{\nu}) = \frac{|C_{p,q}\{e[n]\}|}{|C_{1,1}\{e[n]\}|^{(p+q)/2}} \tag{10}$$

where p and q are non-negative integers, and $p+q \geq 3$, through using gradient type iterative optimization algorithms because all $J_{p,q}(\boldsymbol{\nu})$ are highly nonlinear functions of $\boldsymbol{\nu}$ (without closed-form solutions for the optimum $\boldsymbol{\nu}$). Note that the MIMO-IFC given by (10) include Tugnait's MIMO-IFC [16], [17] for $(p,q) = (2,1)$ and $(p,q) = (2,2)$ as special cases. On the other hand, the iterative MIMO-SEA [22], [23] updates $\boldsymbol{\nu}$ at the Ith iteration by

$$\boldsymbol{\nu}_I = \frac{\tilde{\boldsymbol{R}}^{-1} \cdot \tilde{\boldsymbol{d}}^{(I-1)}}{||\tilde{\boldsymbol{R}}^{-1} \cdot \tilde{\boldsymbol{d}}^{(I-1)}||} \tag{11}$$

where $||\mathbf{a}||$ denotes the Euclidean norm of vector $\mathbf{a}$, and

$$\tilde{\boldsymbol{d}}^{(I-1)} = \mathrm{cum}\{e^{(I-1)}[n] : r, (e^{(I-1)}[n])^* : s-1, \tilde{\boldsymbol{x}}^*[n]\} \tag{12}$$

in which r and $s-1$ are non-negative integers, $r+s \geq 3$, and $e^{(I-1)}[n]$ is the equalizer output obtained at the $(I-1)$th iteration. Two remarks regarding MIMO-IFC and MIMO-SEA are as follows.

R1) In the absence of noise (i.e., SNR $= \infty$), the optimum $e[n] = \alpha_\ell u_\ell[n-\tau_\ell]$ (*perfect equalization*) (i.e., ISI$(e[n]) = 0$) for both MIMO-IFC and MIMO-SEA as $L_1 \to -\infty$ and $L_2 \to \infty$, where $\ell \in \{1,2,\cdots,K\}$, is unknown. For finite SNR and L, $\hat{u}_\ell[n] = e[n]$ is an estimate of $u_\ell[n]$ up to a scale factor and a time delay, and $h_{i\ell}[k] = [\mathbf{H}[k]]_{i\ell}$ (the ith component of the ℓth column of $\mathbf{H}[k]$) can also be estimated as

$$\hat{h}_{i\ell}[k] = \frac{E[x_i[n+k]\hat{u}_\ell^*[n]]}{E[|\hat{u}_\ell[n]|^2]}, \qquad i = 1,2,\cdots P. \tag{13}$$

R2) Although the computationally efficient MIMO-SEA converges at a super-exponential rate for SNR $= \infty$ and sufficiently large N, it may diverge for finite SNR and N. Moreover, with larger computational load than solving the linear equations given by (11) at each iteration, the gradient-type iterative MIMO-IFC algorithms (such as Fletcher–Powell algorithm [29]) always converge slower than the iterative MIMO-SEA for $p+q = r+s$ as $\mathbf{x}[n]$ is real and for $(p,q) = (r,s)$ as $\mathbf{x}[n]$ is complex.

Estimates $\hat{u}_1[n]$, $\hat{u}_2[n], \cdots, \hat{u}_K[n]$ can be obtained by the MIMO-IFC or MIMO-SEA (possibly in a nonsequential order) through an MSC procedure [16] that includes the following two steps at each stage:

S1) Find an input estimate, say $\hat{u}_\ell[n]$ (where ℓ is unknown), using MIMO-IFC or MIMO-SEA and the associated channel estimates $\hat{h}_{i\ell}[n]$, $i = 1,2,\cdots,P$ by (13).

S2) Update $x_i[n]$ by $x_i[n] - \hat{u}_\ell[n] * \hat{h}_{i\ell}[n]$, $i = 1,2,\cdots,P$, i.e., cancel the contribution of $\hat{u}_\ell[n]$ in $\mathbf{x}[n]$.

III. Properties and Fast Algorithms for MIMO-IFC

For ease of later use, let $\mathbf{D}_{p,q}$ be a $K \times K$ diagonal matrix defined as

$$\mathbf{D}_{p,q} = \mathrm{diag}\{C_{p,q}\{u_1[n]\}, \cdots, C_{p,q}\{u_K[n]\}\}. \tag{14}$$

Note that $\mathbf{D}_{1,1} = \mathrm{diag}\{\sigma_{u_1}^2, \cdots, \sigma_{u_K}^2\}$. Prior to presenting analytical results for the performance of the linear equalizer $\mathbf{v}[n]$ associated with MIMO-IFC, let us present the nonblind MIMO minimum mean square error (MIMO-MMSE) equalizer, denoted $\mathcal{V}_{\mathrm{MMSE}}(\omega)$ ($K \times P$ matrix), which will be shown to have some relationship with $\mathbf{v}[n]$ to be presented below. It can be shown by orthogonality principle [30] that

$$\begin{aligned} \mathcal{V}_{\mathrm{MMSE}}^T(\omega) &= (\boldsymbol{V}_{\mathrm{MMSE}}^{[1]}(\omega)\boldsymbol{V}_{\mathrm{MMSE}}^{[2]}(\omega)\cdots\boldsymbol{V}_{\mathrm{MMSE}}^{[K]}(\omega)) \\ &= [\mathcal{R}^T(\omega)]^{-1} \cdot \mathcal{H}^*(\omega) \cdot \mathbf{D}_{1,1} \end{aligned} \tag{15}$$

where $\boldsymbol{V}_{\mathrm{MMSE}}^{[i]}(\omega) = \mathcal{F}\{\boldsymbol{v}_{\mathrm{MMSE}}^{(i)}[n]\}$ is a $P \times 1$ MMSE equalizer

associated with $u_i[n]$, $\mathcal{H}(\omega) = \mathcal{F}\{\mathbf{H}[n]\}$, and

$$\begin{aligned}\mathcal{R}(\omega) &= \mathcal{F}\{\mathbf{R}[k]\} = \mathcal{F}\{E[\mathbf{x}[n]\mathbf{x}^H[n-k]]\} \\ &= \mathcal{H}(\omega)\cdot\mathbf{D}_{1,1}\cdot\mathcal{H}^H(\omega) + \mathcal{F}\{\mathbf{Q}[k]\}. \end{aligned} \tag{16}$$

Three properties of the optimum $\mathbf{v}[n]$ for any SNR are proposed as follows.

Property 1: As the noise $\mathbf{w}[n]$ is zero-mean spatially independent (i.e., $[\mathbf{Q}[k]]_{il} = 0$ for $i \neq l$), the optimum overall channel impulse responses $s_k[n]$ given by (4), $k = 1, \cdots, K$ are linear phase for finite L, i.e., their phase responses are given by

$$\arg[S_k(\omega)] = \omega\tau_k + \xi_k, \quad \forall\omega \in [-\pi, \pi) \tag{17}$$

where $S_k(\omega) = \mathcal{F}\{s_k[n]\}$, τ_k, and ξ_k are real constants. □

Property 2: Let

$$g_{pqk}[n] = s_k^p[n](s_k^*[n])^{q-1} \tag{18}$$

$$\begin{aligned}\boldsymbol{G}_{p,q}(\omega) &= (G_{pq1}(\omega) = \mathcal{F}\{g_{pq1}[n]\}, \cdots, G_{pqK}(\omega) \\ &= \mathcal{F}\{g_{pqK}[n]\})^T. \end{aligned} \tag{19}$$

The optimum $\boldsymbol{V}(\omega) = \mathcal{F}\{\mathbf{v}[n]\}$ for $L_1 \to -\infty$ and $L_2 \to \infty$ is related to $\mathcal{V}_{\mathrm{MMSE}}(\omega)$ by

$$\boldsymbol{V}(\omega) = \mathcal{V}_{\mathrm{MMSE}}^T(\omega)\cdot\tilde{\boldsymbol{G}}(\omega) \tag{20}$$

where

$$\tilde{\boldsymbol{G}}(\omega) = \mathbf{D}_{1,1}^{-1}(\alpha_{q,p}\mathbf{D}_{q,p}\boldsymbol{G}_{q,p}(\omega) + \alpha_{p,q}\mathbf{D}_{p,q}\boldsymbol{G}_{p,q}(\omega)) \tag{21}$$

in which

$$\alpha_{p,q} = \frac{q\cdot C_{1,1}\{e[n]\}}{(p+q)\cdot C_{p,q}\{e[n]\}}. \tag{22}$$

□

Property 3: The optimum $\mathbf{v}[n]$ with finite L, and the one obtained by the MIMO-SEA are the same (up to a scale factor) for $p+q = r+s \geq 3$ as $\mathbf{x}[n]$ is real and for $p = q = r = s \geq 2$ as $\mathbf{x}[n]$ is complex. □

The following Lemma is needed in the proof of Property 2.

Lemma 1:

$$C_{p,q}\{e[n]\} = C_{q,p}^*\{e[n]\} \tag{23}$$

$$\frac{\partial C_{p,q}\{e[n]\}}{\partial\boldsymbol{\nu}^*} = q\cdot\mathrm{cum}\{e[n]:p, e^*[n]:q-1, \tilde{\boldsymbol{x}}^*[n]\} \tag{24}$$

□

The proofs for Property 1, Lemma 1, and Properties 2 and 3 are presented in Appendices A, B, C, and D, respectively.

Substituting (7) and (8) into (10) yields

$$J_{p,q}(\mathbf{v}[n]) = \frac{\left|\sum_{i=1}^{K} C_{p,q}\{u_i[n]\}\left(\sum_{n=-\infty}^{\infty} s_i^p[n](s_i^*[n])^q\right)\right|}{\left|\sum_{i=1}^{K}\sigma_{u_i}^2\left(\sum_{n=-\infty}^{\infty}|s_i[n]|^2\right) + r_{ww}[0]\right|^{(p+q)/2}}. \tag{25}$$

By Property 2, the theoretically optimum (true) $\mathbf{v}[n]$ by maximizing $J_{p,q}(\mathbf{v}[n])$ given by (25) must be the same as the one obtained through the relation given by (20). Therefore, to verify Property 2 by simulation, we need to compute the true $\mathbf{v}[n]$ through the relation given by (20) and then compare it with the obtained estimate $\hat{\mathbf{v}}[n]$ using simulation data. The following iterative FFT-based algorithm that is also an extension of the one reported in [12] for the SISO case is proposed for obtaining the true $\mathbf{v}[n]$.

Algorithm 1

S1) Set $i = 0$. Choose an initial condition $\mathbf{v}^{(0)}[n]$ for $\mathbf{v}[n]$ and a convergence tolerance $\epsilon > 0$.

S2) Set $i = i+1$. Compute the $\mathcal{L}$-point DFT $\boldsymbol{V}^{(i-1)}(\omega_k = 2\pi k/\mathcal{L})$, $k = 0, 1, \cdots, \mathcal{L}-1$ of $\mathbf{v}^{(i-1)}[n]$. Compute $\boldsymbol{S}^{(i-1)}(\omega_k) = \mathcal{H}^T(\omega_k)\boldsymbol{V}^{(i-1)}(\omega_k)$ by (4), and then obtain its $\mathcal{L}$-point inverse DFT $\mathbf{s}^{(i-1)}[n]$.

S3) Compute $\boldsymbol{G}_{p,q}(\omega_k)$ and $\boldsymbol{G}_{q,p}(\omega_k)$ using (18) and (19) with $\mathbf{s}[n] = \mathbf{s}^{(i-1)}[n]$. Then, compute $\tilde{\boldsymbol{G}}(\omega_k)$ using (21).

S4) Compute $\tilde{\boldsymbol{V}}(\omega_k) = \mathcal{V}_{\mathrm{MMSE}}^T(\omega_k)\tilde{\boldsymbol{G}}(\omega_k)$ by (20) followed by its $\mathcal{L}$-point inverse DFT $\tilde{\mathbf{v}}[n]$. Then, obtain $\mathbf{v}^{(i)}[n] = \tilde{\mathbf{v}}[n]/\sqrt{\sum_{j=1}^{P}\sum_n|\tilde{v}_j[n]|^2}$. If $J_{p,q}(\mathbf{v}^{(i)}[n]) > J_{p,q}(\mathbf{v}^{(i-1)}[n])$, go to S6).

S5) Update $\mathbf{v}^{(i)}[n]$ through a gradient type optimization algorithm.

S6) If $\sum_{j=1}^{P}\sum_n|v_j^{(i)}[n] - v_j^{(i-1)}[n]|^2 > \epsilon$, then go to S2); otherwise, the true $\mathbf{v}[n] = \mathbf{v}^{(i)}[n]$ is obtained.

Note that Algorithm 1, which is never an MIMO blind deconvolution algorithm, is merely an iterative algorithm that requires the channel response $\mathcal{H}(\omega)$, variances $\sigma_{u_i}^2$, and $(p+q)$th-order cumulants $C_{p,q}\{u_i[n]\}$ of input signals and noise covariance matrix $\mathbf{Q}[k]$ to compute the optimum $\mathbf{v}[n]$ associated with the MIMO-IFC $J_{p,q}(\mathbf{v}[n])$ given by (25). However, it is never limited by the length of $\mathbf{v}[n]$ as long as the DFT length $\mathcal{L}$ is chosen sufficiently large such that aliasing effects on the resultant $\mathbf{v}[n]$ is negligible. Moreover, the convergence of Algorithm 1 can be guaranteed because $J_{p,q}(\mathbf{v}^{(i)}[n])$ (which is bounded) increases at each iteration, and S5) is rarely performed.

Based on Property 3 and R2), a fast iterative MIMO blind deconvolution algorithm using MIMO-IFC is proposed as follows.

Algorithm 2

Given $\boldsymbol{\nu}_{I-1}$ and $e^{(I-1)}[n]$ obtained at the $(I-1)$th iteration, $\boldsymbol{\nu}_I$ at the Ith iteration is obtained by the following two steps.

S1) As the MIMO-SEA, obtain $\boldsymbol{\nu}_I$ by (11) with $r+s = p+q$ as $\mathbf{x}[n]$ is real and with $r = s = p = q$ as $\mathbf{x}[n]$ is complex, and obtain the associated $e^{(I)}[n]$.

S2) If $J_{p,q}(\boldsymbol{\nu}_I) > J_{p,q}(\boldsymbol{\nu}_{I-1})$, go to the next iteration; otherwise, update $\boldsymbol{\nu}_I$ through a gradient-type optimization algorithm such that $J_{p,q}(\boldsymbol{\nu}_I) > J_{p,q}(\boldsymbol{\nu}_{I-1})$, and obtain the associated $e^{(I)}[n]$.

As $\mathbf{x}[n]$ is complex for $p = q = r = s$ and $\mathbf{x}[n]$ is real for $p+q = r+s$, it can be shown that

$$\left.\frac{\partial J_{p,q}(\boldsymbol{\nu})}{\partial\boldsymbol{\nu}}\right|_{\boldsymbol{\nu}=\boldsymbol{\nu}_{I-1}} \propto \frac{1}{C_{p,q}\{e^{(I-1)}[n]\}}\cdot(\tilde{\boldsymbol{d}}^{(I-1)})^* - \frac{1}{C_{1,1}\{e^{(I-1)}[n]\}}\cdot(\tilde{\boldsymbol{R}}\boldsymbol{\nu}_{I-1})^* \tag{26}$$

where $\tilde{\boldsymbol{d}}^{(I-1)}$ has been obtained in S1) of Algorithm 2 [see (11)], and $\tilde{\boldsymbol{R}}$ is the same at each iteration, indicating simple and straightforward computation for obtaining $\partial J_{p,q}(\boldsymbol{\nu})/\partial \boldsymbol{\nu}$ in (S2) of Algorithm 2. The proof of (26) is given in Appendix E. Let us conclude this section with the following remark.

R3) Algorithm 2 performs as a fast gradient type MIMO-IFC algorithm with convergence speed, computational load, and ISI similar to those of MIMO-SEA due to the step S1) of Algorithm 2. Therefore, Properties 1, 2, and 3 also apply to the optimum inverse filter obtained by Algorithm 2. Moreover, the convergence of Algorithm 2 can be guaranteed because $J_{p,q}(\boldsymbol{\nu}_I)$ (which is bounded) increases at each iteration due to step S2) of Algorithm 2.

IV. Blind Equalization for DS/CDMA Systems Using MIMO-IFC

Blind deconvolution of MIMO systems in multiuser communications [1]–[4], [18], [31]–[34] includes suppression of MAI and ISI that are crucial to the receiver design of multiuser communications systems. In this section, Algorithm 2 is applied to the suppression of MAI and ISI for multiuser asynchronous DS/CDMA systems. Next, let us briefly review the MIMO model for asynchronous DS/CDMA systems.

A. MIMO Model for Asynchronous DS/CDMA Systems

For a K-user asynchronous DS/CDMA communication system in the absence of multipath, the received continuous time signal is given by [1]

$$x(t)=\sum_{k=1}^{K}\sum_{n=0}^{N-1}\overline{A}_k u_k[n]\overline{s}_k(t-nT-\overline{\tau}_k)+\sigma_{\overline{w}}\overline{w}(t) \tag{27}$$

where

T	symbol period;
$\overline{A}_k$	amplitude;
$u_k[n]$	symbol sequence;
N	length of symbol sequence;
$\overline{\tau}_k \le T$	propagation delay associated with user k;
$\overline{w}(t)$	zero-mean Gaussian noise with unit variance;
$\overline{s}_k(t)$	signature waveform of unit energy associated with user k given by

$$\overline{s}_k(t)=\frac{1}{\sqrt{T}}\sum_{n=0}^{\mathcal{P}-1}c_k[n]\overline{p}(t-nT_c) \tag{28}$$

where

$\mathcal{P}$	spreading gain;
T_c	chip period ($=T/\mathcal{P}$);
$c_k[n]$	binary pseudo random sequence of $\{+1,-1\}$;
$\overline{p}(t)$	rectangular chip pulse of magnitude equal to unity.

Assume that continuous-time multipath channel for user k is given by

$$h_k(t)=\sum_{m=1}^{M_k}\tilde{A}_{km}\delta(t-\tilde{\tau}_{km}) \tag{29}$$

where $\tilde{A}_{km}$ and $\tilde{\tau}_{km}$ are attenuation factor and time delay for the mth path associated with user k, respectively, and M_k is the number of paths for user k. Then, the received signal can be expressed as

$$x(t)=\sum_{k=1}^{K}\sum_{n=0}^{N-1}\sum_{m=1}^{M_k}A_{km}u_k[n]\cdot\overline{s}_k(t-nT-\tau_{km})+\sigma_{\overline{w}}\overline{w}(t) \tag{30}$$

where $A_{km}=\overline{A}_k\tilde{A}_{km}$ and $\tau_{km}=\overline{\tau}_k+\tilde{\tau}_{km}$.

Assume that $0\le\tau_{k1}\le\tau_{k2}\le\cdots\le\tau_{kM_k}\le T+\tau_{k1}$, $\forall k$, i.e., the delay spread of all the channels $\tau_{kM_k}-\tau_{k1}\le T$, $\forall k$ [3], [32], [34] and $0\le\tau_{11}\le\tau_{21}\le\cdots\le\tau_{K1}\le T$, i.e., the first propagation delay $\tau_{k1}\le T$, $\forall k$. Let $x_{km}[n]$ be the signature waveform matched filter output associated with the mth path of the kth user assuming perfect synchronization, and let $w_{km}[n]$ be the noise term in $x_{km}[n]$ due to $\overline{w}(t)$, i.e.,

$$x_{km}[n]=\int_{nT+\tau_{km}}^{(n+1)T+\tau_{km}}x(t)\overline{s}_k^*(t-nT-\tau_{km})\,dt \tag{31}$$

$$w_{km}[n]=\sigma_{\overline{w}}\int_{nT+\tau_{km}}^{(n+1)T+\tau_{km}}\overline{w}(t)\overline{s}_k^*(t-nT-\tau_{km})\,dt. \tag{32}$$

It can be easily shown that

$$\begin{aligned}\mathbf{x}_k[n]&=(x_{k1}[n],x_{k2}[n],\cdots,x_{k\mathcal{M}_k}[n])^T\\&=\tilde{\mathbf{H}}^{(k)}[n]*\mathbf{u}[n]+\mathbf{w}_k[n]\\&=\left(\sum_{m=1}^{M_k}\mathbf{H}_m^{(k)}[n]\mathbf{A}_m\right)*\mathbf{u}[n]+\mathbf{w}_k[n]\end{aligned} \tag{33}$$

where $1\le\mathcal{M}_k\le M_k$, $\mathbf{A}_m=\mathrm{diag}\{A_{1m},A_{2m},\cdots,A_{Km}\}$, $\mathbf{w}_k[n]$ is colored Gaussian noise, and $\mathbf{H}_m^{(k)}[n]$ is an $\mathcal{M}_k\times K$ matrix with the (l,j)th element

$$[\mathbf{H}_m^{(k)}[n]]_{lj}=\begin{cases}\rho_{ljkm}^{(n)}, & n=-2,-1,\cdots,2\\ 0, & \text{otherwise}\end{cases} \tag{34}$$

in which

$$\rho_{ljkm}^{(n)}=\int_0^T\overline{s}_k^*(t)\overline{s}_j(t+nT+\tau_{kl}-\tau_{jm})\,dt. \tag{35}$$

Then, from (33), it can be easily obtained that

$$\mathbf{x}[n]=(\mathbf{x}_1^T[n],\mathbf{x}_2^T[n],\cdots,\mathbf{x}_K^T[n])^T=\mathbf{H}[n]*\mathbf{u}[n]+\mathbf{w}[n] \tag{36}$$

where

$$\begin{aligned}\mathbf{u}[n]&=(u_1[n],u_2[n],\cdots,u_K[n])^T\\\mathbf{w}[n]&=(\mathbf{w}_1^T[n],\mathbf{w}_2^T[n],\cdots,\mathbf{w}_K^T[n])^T\end{aligned}$$

and $\mathbf{H}[n]$ is an $\mathcal{M}\times K$ system given by

$$\mathbf{H}[n]=((\tilde{\mathbf{H}}^{(1)}[n])^T(\tilde{\mathbf{H}}^{(2)}[n])^T\cdots(\tilde{\mathbf{H}}^{(K)}[n])^T)^T \tag{37}$$

where $\mathcal{M}=\sum_{i=1}^{K}\mathcal{M}_i$.

Moreover, the vector noise $\mathbf{w}[n]$ is zero mean colored Gaussian whose covariance matrix is a $K \times K$ block matrix given by

$$\mathbf{Q}[k] = E[\mathbf{w}[n]\mathbf{w}^H[n-k]] = \{\mathbf{Q}_{i,j}[k]\}_{K\times K} \tag{38}$$

in which $\mathbf{Q}_{i,j}[k] = E[\mathbf{w}_i[n]\mathbf{w}_j^H[n-k]]$ is an $\mathcal{M}_i \times \mathcal{M}_j$ matrix with the (l,m)th entry given by

$$[\mathbf{Q}_{i,j}[k]]_{lm} = \sigma_w^2 \int_0^T \overline{s}_i^*(t)\overline{s}_j(t+kT+\tau_{il}-\tau_{jm})\,dt. \tag{39}$$

One worthy remark regarding the MIMO model given by (36) for asynchronous DS/CDMA systems is as follows.

R4) The impulse response matrices $\tilde{\mathbf{H}}^{(k)}[n]$ given by (33) and $\mathbf{H}[n]$ given by (37) are of length five. $\tilde{\mathbf{H}}^{(k)}[n]$ can also be expressed in the following form:

$$\tilde{\mathbf{H}}^{(k)}[n] = (\tilde{\mathbf{0}}_1 \cdots \tilde{\mathbf{0}}_{k-1}\boldsymbol{\mathcal{A}}_k\tilde{\mathbf{0}}_{k+1}\cdots\tilde{\mathbf{0}}_K)\cdot\delta[n] + \overline{\mathbf{S}}^{(k)}[n] \tag{40}$$

where $\boldsymbol{\mathcal{A}}_k = (A_{k1},\cdots,A_{k\mathcal{M}_k})^T$ and $\tilde{\mathbf{0}}_i$ are $\mathcal{M}_k \times 1$ zero vectors for all i. Under good power control, the energy of each component of the $\mathcal{M}_k \times K$ matrix $\overline{\mathbf{S}}^{(k)}[n]$ in (40) can be much smaller than $|A_{kl}|^2$ for all $l = 1,\cdots,\mathcal{M}_k$ as K is not very large, due to low cross correlation between waveforms $\overline{s}_k(t)$ and $\overline{s}_j(t)$ for all $k \neq j$ in general.

B. MAI and ISI Suppression Using Algorithm 2

The proposed Algorithm 2 is an iterative blind deconvolution algorithm that can be employed to process the received discrete-time signal $\mathbf{x}[n]$ modeled by (36) without the need of information of channel, signal magnitudes (or powers), and noise statistics as long as synchronization of the received signal $x(t)$ with at least one path is achieved.

Assume that user j is the user of interest. Because of error propagation in the MSC procedure, we prefer to obtain $e[n] = \hat{u}_j[n]$ at the first stage (without going through the K stages) of the MSC procedure. By our experience, the initial condition

$$\mathbf{v}^{(0)}[n] = (\mathbf{0}_1^T\cdots\mathbf{0}_{j-1}^T\boldsymbol{\zeta}_j^H\mathbf{0}_{j+1}^T\cdots\mathbf{0}_K^T)^T\cdot\delta[n-n_0] \tag{41}$$

where $L_1 \le n_0 \le L_2$, $\mathbf{0}_i$ is an $\mathcal{M}_i \times 1$ zero vector, and $\boldsymbol{\zeta}_j$ ($\mathcal{M}_j \times 1$ column vector) is the principal eigenvector of $E[\mathbf{x}_j[n]\mathbf{x}_j^H[n]]$ [35], can usually lead Algorithm 2 to $e[n] = \hat{u}_j[n]$ at the first stage of the MSC procedure as power control is fine, and K is not very large. The reason for this is as follows. Associated with $\mathbf{v}^{(0)}[n]$ given by (41), one can easily see that $e^{(0)}[n] = \boldsymbol{\zeta}_j^H\mathbf{x}_j[n-n_0]$ and

$$\begin{aligned}\mathbf{s}^{(0)}[n] &= \mathbf{H}^T[n] * \mathbf{v}^{(0)}[n] \quad \text{[by (4)]}\\ &= \boldsymbol{\zeta}_j^H\boldsymbol{\mathcal{A}}_j\cdot\boldsymbol{\varepsilon}_j\cdot\delta[n-n_0] + (\boldsymbol{\zeta}_j^H\overline{\mathbf{S}}^{(j)}[n-n_0])^T\\ &\qquad \text{[by (37), (40), and (41)].}\end{aligned} \tag{42}$$

Note that ISI($e^{(0)}[n]$) is usually small since the energy of each entry of the second term on the right-hand side of (42) is much smaller than $|\boldsymbol{\zeta}_j^H\boldsymbol{\mathcal{A}}_j|$ by R4). Consequently, the user j will be locked in the ensuing iterations by forcing ISI to decrease. Remark that with the initial condition $\mathbf{v}^{(0)}[n]$ given by (41), it is not necessary that $\hat{u}_j[n]$ be obtained as user signal powers are very unbalanced or the number of users is large.

V. Simulation Results

Three simulation examples are to be presented. The first example considers a 2×2 LTI system, and Examples 2 and 3 consider a two-user and an eight-user asynchronous DS/CDMA systems in multipath, respectively. Example 1 is for verifying Properties 1 and 3 and supporting the efficacy and robustness of Algorithm 2. Example 2 is basically for verifying Property 2, and Example 3 is for supporting that Algorithm 2 is effective for MAI and ISI suppression. In the three examples, the input signals $u_i[n]$, $i = 1,\cdots,K$ were assumed to be equally probable binary random sequences of $\{+1,-1\}$, and the synthetic data $\mathbf{x}[n]$ were generated for different values of SNR defined as

$$\text{SNR} = \frac{E[\|\mathbf{x}[n]-\mathbf{w}[n]\|^2]}{E[\|\mathbf{w}[n]\|^2]}. \tag{43}$$

Next, let us turn to Example 1.

A. Example 1

1) Properties 1 and 3 and Efficacy of Algorithm 2: A two-input two-output system

$$\mathcal{H}(z) = \begin{bmatrix} b - 0.3227z^{-1} + 0.6455z^{-2} - 0.3227z^{-3} & 0.6140 + 0.3684z^{-1} \\ 0.3873z^{-1} + 0.8391z^{-2} + 0.3227z^{-3} & -0.2579z^{-1} - 0.6140z^{-2} + 0.8842z^{-3} \\ & +0.4421z^{-4} + 0.2579z^{-6} \end{bmatrix} \tag{44}$$

with $b = 0.6455$, which is taken from [16], was used. The noise vector $\mathbf{w}[n]$ was assumed to be spatially independent and temporally white Gaussian. The synthetic data $\mathbf{x}[n]$ for $N = 900$ and $\text{SNR}_k = E[|x_k[n]-w_k[n]|^2]/E[|w_k[n]|^2] = \text{SNR} = 15$ dB, $k = 1, 2$ were processed by the equalizer $\mathbf{v}[n]$ of length $L = 30$ ($L_1 = 0$ and $L_2 = 29$) associated with MIMO-IFC using the iterative Fletcher–Powell algorithm [29] (a gradient-type iterative algorithm), MIMO-SEA with $r = s = 2$, and Algorithm 2 with $p = q = r = s = 2$, respectively. The initial condition $\boldsymbol{\nu}_0$ for the three algorithms was associated with $\mathbf{v}^{(0)}[n] = (\boldsymbol{\varepsilon}_1 + \boldsymbol{\varepsilon}_2)\delta[n-14]$ (i.e., $v_1^{(0)}[n] = v_2^{(0)}[n] = \delta[n-14]$) for the first stage and $\mathbf{v}^{(0)}[n] = \boldsymbol{\varepsilon}_1\delta[n-14]$ (i.e., $v_1^{(0)}[n] = \delta[n-14]$ and $v_2^{(0)}[n] = 0$) for the second stage of the MSC procedure.

Thirty independent realizations of the optimum $s_1[n]$ and the associated 30 ISIs versus iteration number obtained at the first stage of the MSC procedure (associated with $e[n] = \hat{u}_1[n]$) are shown in Fig. 1(a)–(f) using the three algorithms, respectively. Fig. 1(a), (c), and (e) show $s_1[n]$s associated with MIMO-IFC, MIMO-SEA, and Algorithm 2, respectively. Fig. 1(b), (d), and (f) shows ISIs associated with MIMO-IFC, MIMO-SEA, and Algorithm 2, respectively. One can see, from Fig. 1, that the

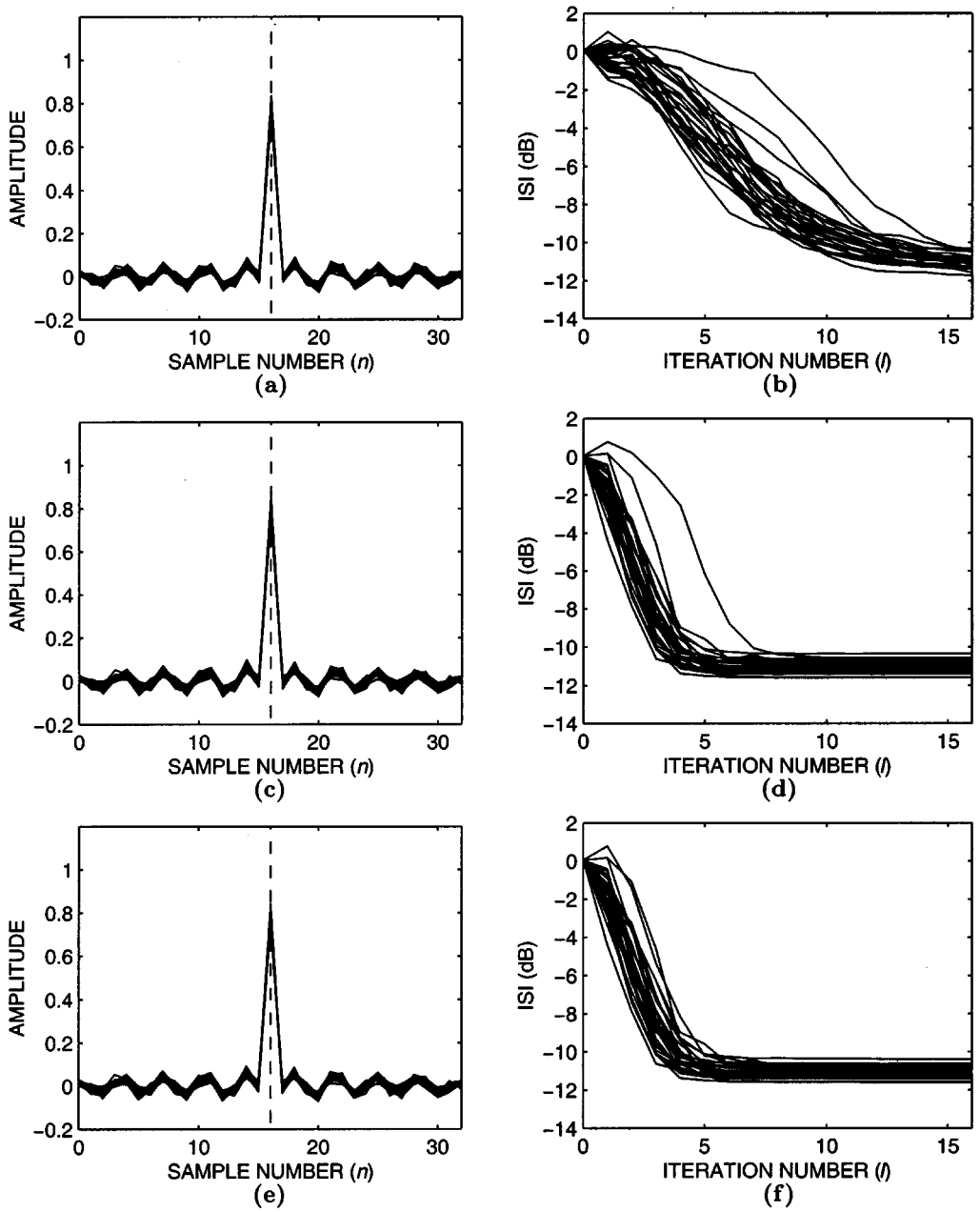

Fig. 1. Simulation results of Example 1. Thirty $s_1[n]$s and ISIs versus iteration number I at the first stage of the MSC procedure for $b = 0.6455$. (a) $s_1[n]$ and (b) ISI associated with MIMO-IFC for $p = q = 2$ using Fletcher-Powell Algorithm. (c) $s_1[n]$ and (d) ISI associated with MIMO-SEA for $r = s = 2$. (e) $s_1[n]$ and (f) ISI associated with Algorithm 2 for $p = q = 2$.

resultant $s_1[n]$s are linear phase and they are similar for the three algorithms thus verifying Properties 1 and 3, whereas the convergence speed for the proposed Algorithm 2 is basically the same as that of MIMO-SEA and faster than the MIMO-IFC using the Fletcher-Powell algorithm [see R2)]. The results for $s_2[n]$ obtained at the first stage of the MSC procedure are omitted here since they are close to zero. The corresponding results for $s_2[n]$ and ISI obtained at the second stage of the MSC procedure (associated with $e[n] = \hat{u}_2[n]$) are shown in Fig. 2(a)–(f) without including the results for $s_1[n]$ since they are close to zero. These results also support Properties 1 and 3, but the MIMO-SEA fails to converge in one realization [see Fig. 2(d)] with the associated $s_2[n]$ not approximating a delta function [see Fig. 2(c)] [see also R2)]. Algorithm 2 outperforms the other two algorithms because the former converges as fast as the MIMO-SEA in all 30 realizations (without any divergence) and converges faster than the MIMO-IFC using the Fletcher-Powell algorithm.

Moreover, it can be observed from Figs. 1(b), (d), and (f) and 2(b), (d), and (f) that some ISIs increase at the beginning iterations for the three algorithms, and then they decrease rapidly in the ensuing iterations for the MIMO-SEA and Algorithm 2. Some ISIs associated with the MIMO-SEA and Algorithm 2 are exactly the same because only the step S1) of the latter (which is exactly the MIMO-SEA) was performed in obtaining these results. Some ISIs associated with the MIMO-SEA do not decrease fast, whereas Algorithm 2 can always make them decrease fast by forcing $J_{2,2}(\boldsymbol{\nu})$s to increase in the step S2).

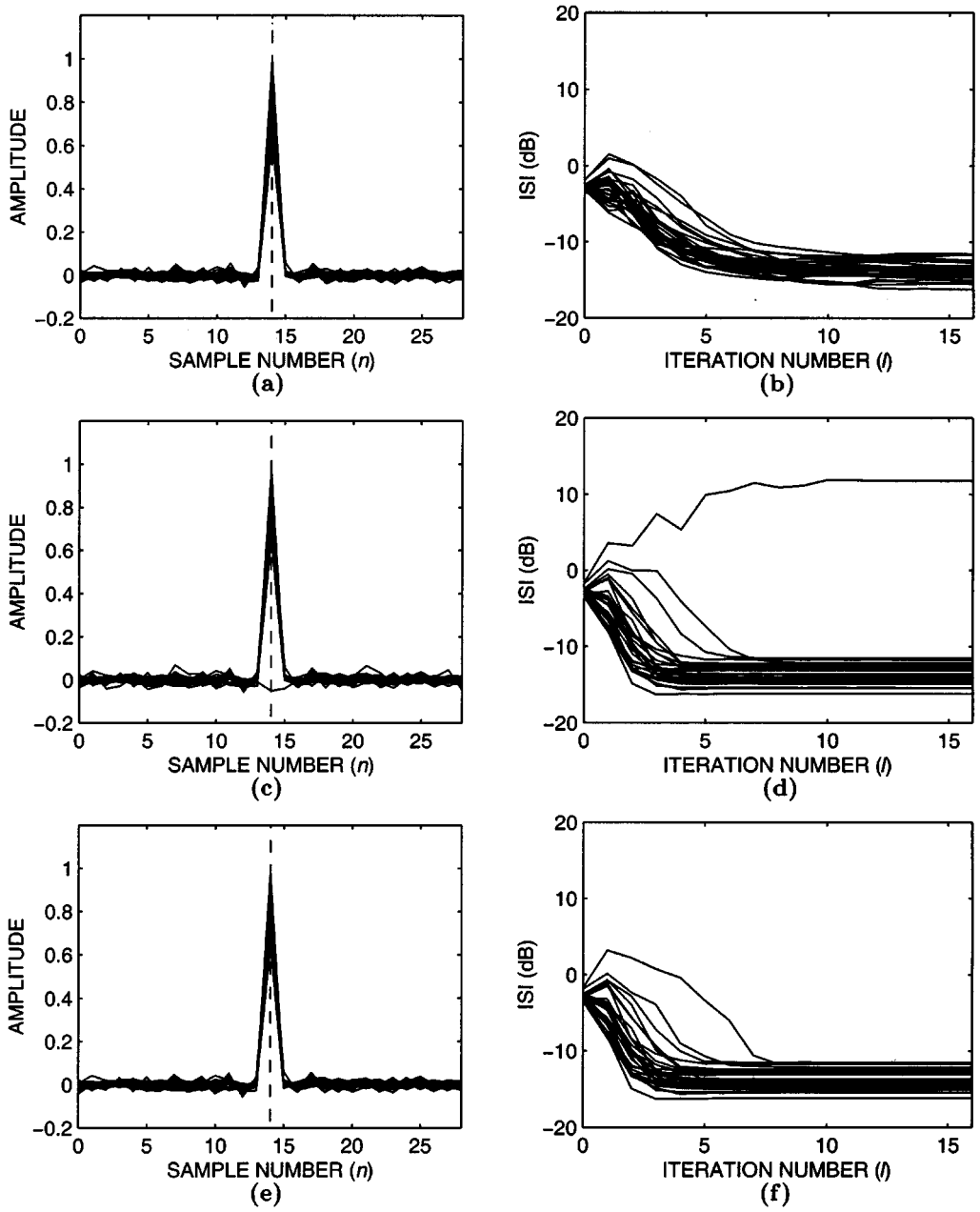

Fig. 2. Simulation results of Example 1. Thirty $s_2[n]$s and ISIs versus iteration number I at the second stage of the MSC procedure for $b = 0.6455$. (a) $s_2[n]$ and (b) ISI associated with MIMO-IFC for $p = q = 2$ using Fletcher-Powell algorithm. (c) $s_2[n]$ and (d) ISI associated with MIMO-SEA for $r = s = 2$. (e) $s_2[n]$ and (f) ISI associated with Algorithm 2 for $p = q = 2$.

Moreover, the resultant ISIs are similar for both MIMO-SEA and Algorithm 2. These results are consistent with R3).

2) Robustness Test of Algorithm 2: In the simulation, the synthetic data $\mathbf{x}[n]$ were generated through the same procedure as in part 1 for $b = -1$, -0.5, 0, 0.5, 1 [see (44)], respectively, and then processed by Algorithm 2 with the same parameters and initial condition for the inverse filter associated with MIMO-IFC as used in part 1.

Thirty independent realizations of ISIs versus iteration number obtained at the first stage of the MSC procedure (associated with $c[n] = \hat{u}_1[n]$) are shown in Fig. 3(a)–(e) for $b = -1$, -0.5, 0, 0.5, and 1, respectively. Fig. 4(a)–(e) shows the corresponding results obtained at the second stage of the MSC procedure (associated with $c[n] = \hat{u}_2[n]$). One can see, from Figs. 3 and 4, that all the ISIs converge fast (spending within seven iterations) to the final small ISIs that depend on the value of the system parameter b. These simulation results verify the robustness of Algorithm 2.

B. Example 2

In this example, an asynchronous DS/CDMA channel for two users ($K = 2$), each with three paths ($M_1 = M_2 = 3$), was considered. The users' spreading codes $c_j[n]$ are Gold codes of length $\mathcal{P} = 31$. The channel parameters used were $A_{km} = 1$, $k = 1, 2$, $m = 1, 2, 3$, $(\tau_{11}, \tau_{12}, \tau_{13}) = (0, 5T_c, 8T_c)$, and $(\tau_{21}, \tau_{22}, \tau_{23}) = (4T_c, 11T_c, 13T_c)$. The synthetic data $\mathbf{x}[n]$ for $\mathcal{M}_1 = \mathcal{M}_2 = 1$, $N = 1500$ and SNR $= 20$ dB were processed by Algorithm 2 with $p = q = r = s = 2$ for which the equalizer

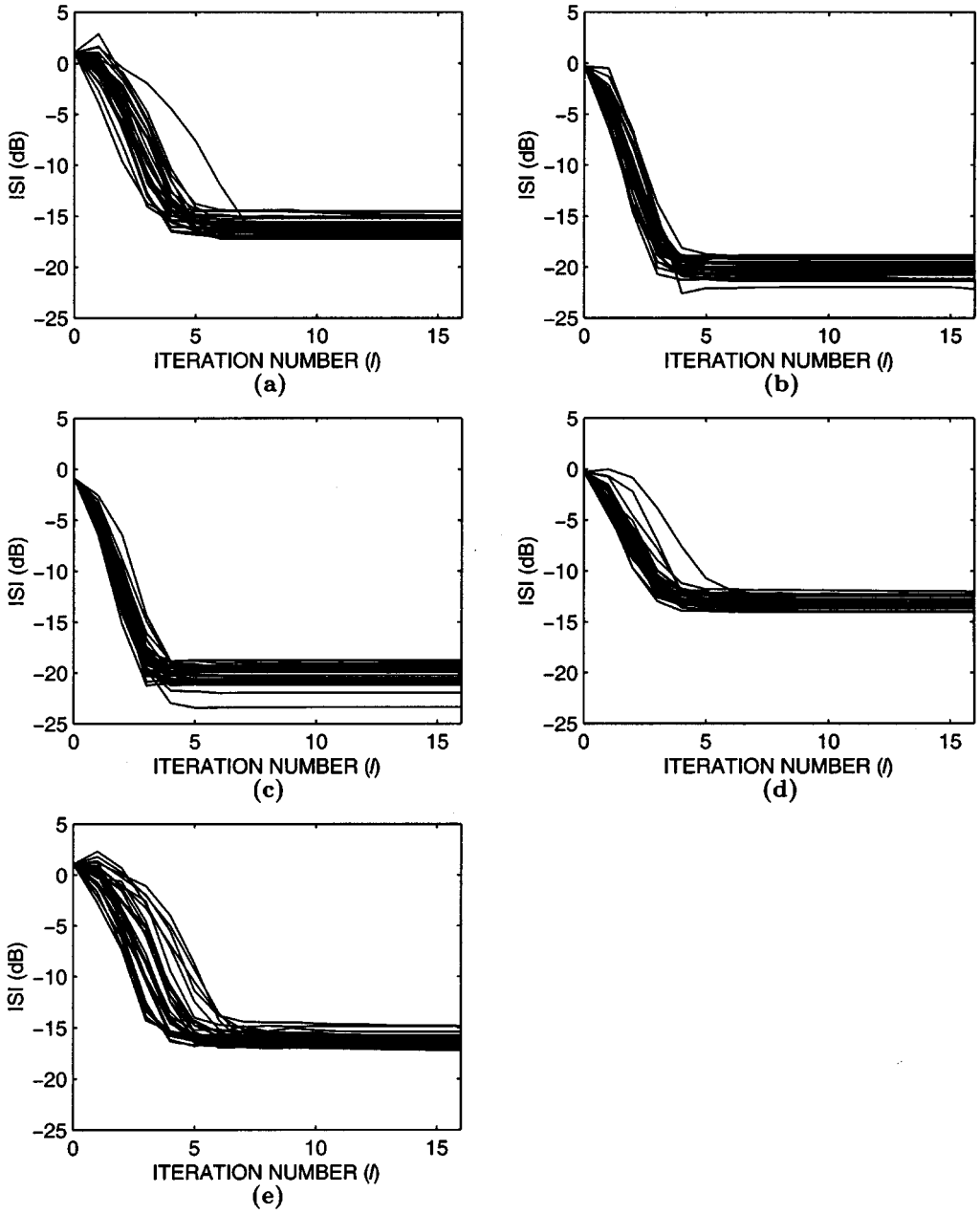

Fig. 3. Simulation results of Example 1. Thirty ISIs versus iteration number I at the first stage of the MSC procedure associated with Algorithm 2 for (a) $b = -1$, (b) $b = -0.5$, (c) $b = 0$, (d) $b = 0.5$, and (e) $b = 1$, respectively.

$\mathbf{v}[n]$ of length $L = 10$ ($L_1 = 0$ and $L_2 = 9$) was used. On the other hand, the theoretical (true) $\mathbf{v}[n] = (v_1[n], v_2[n])^T$ associated with $e[n] = \hat{u}_1[n]$ and that associated with $e[n] = \hat{u}_2[n]$ were obtained by Algorithm 1 with $\epsilon = 10^{-4}$ and $\mathcal{L} = 32$. The initial condition $\mathbf{v}^{(0)}[n]$ given by (41) with $n_0 = 4$ for the chosen j was used to initialize Algorithms 1 and 2 for estimating $u_j[n]$ without involving the MSC procedure.

Simulation results associated with $e[n] = \hat{u}_1[n]$ are shown in Fig. 5. Thirty independent estimates $\hat{v}_1[n]$ and $\hat{v}_2[n]$ are shown in Fig. 5(a) and (c), respectively; the true $v_1[n]$ and $v_2[n]$ are shown in Fig. 5(b) and (d), respectively; the associated 30 ISIs versus iteration number are shown in Fig. 5(e); the true overall channel responses $s_1[n]$ (dash line) and $s_2[n]$ (dotted line) (after equalization) are shown in Fig. 5(f). The corresponding results associated with $e[n] = \hat{u}_2[n]$ are shown in Fig. 6(a)–(f), respectively. From Figs. 5(a)–(d) and 6(a)–(d), one can see that all the obtained optimum $\hat{v}_1[n]$ and $\hat{v}_2[n]$ are very close to the true $v_1[n]$ and $v_2[n]$, respectively. From Figs. 5(e) and 6(e), one can see that all the ISIs converge fast (by spending around two iterations) with the resultant ISI below -35 dB. From Figs. 5(f) and 6(f), one can see that the overall channel impulse response $\mathbf{s}[n] \simeq \boldsymbol{\varepsilon}_1 \delta[n-4]$ for the former and $\mathbf{s}[n] \simeq \boldsymbol{\varepsilon}_2 \delta[n-4]$ for the latter, respectively. These simulation results verify Property 2 of MIMO-IFC and support the fact that Algorithm 2 works well. As a final remark, Algorithm 1 also converges fast (by spending two iterations) in obtaining the true $\mathbf{v}[n]$ shown in Fig. 5(b) and (d) and Fig. 6(b) and (d) without involving S5).

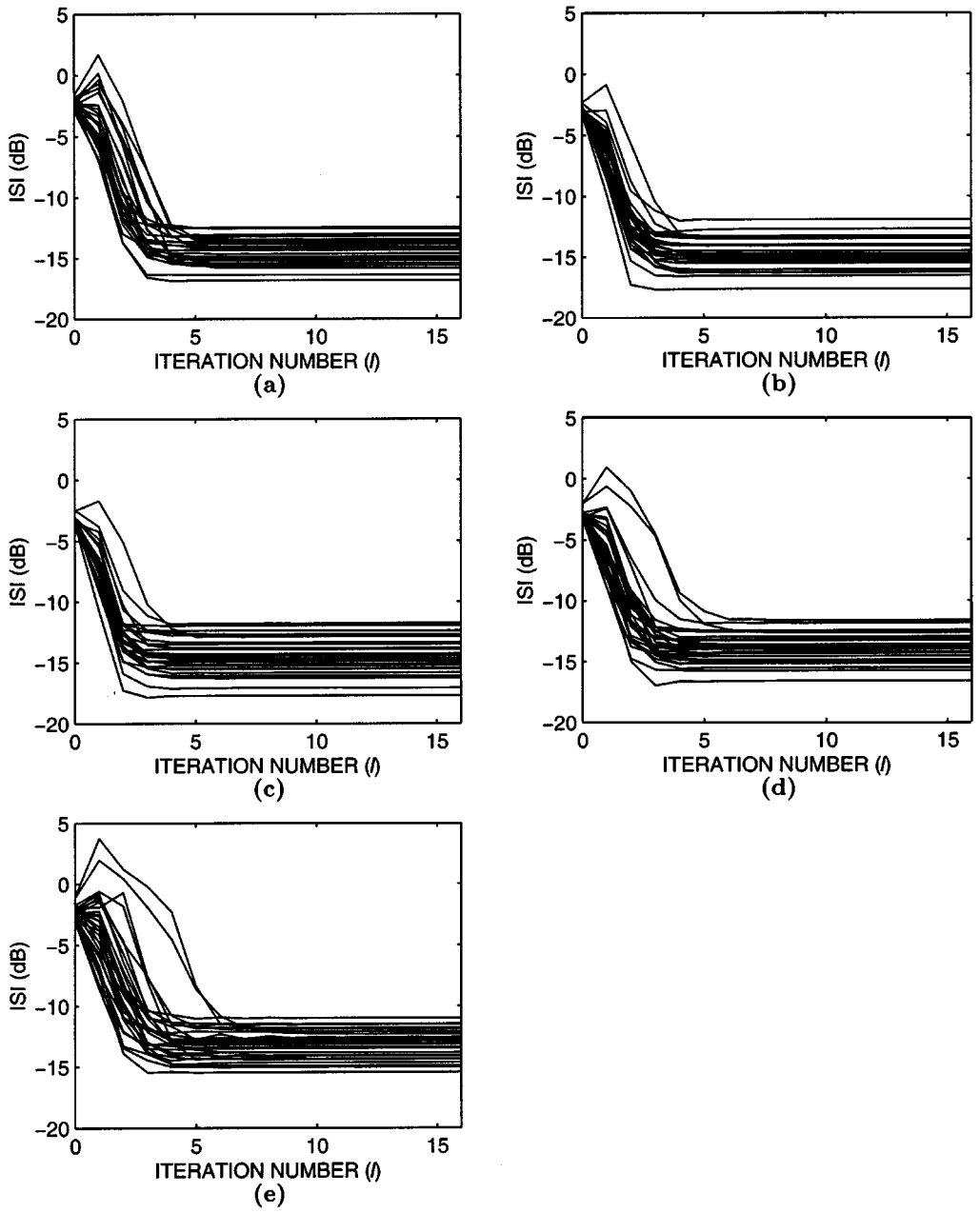

Fig. 4. Simulation results of Example 1. Thirty ISIs versus iteration number I at the second stage of the MSC procedure associated with Algorithm 2 for (a) $b = -1$, (b) $b = -0.5$, (c) $b = 0$, (d) $b = 0.5$, and (e) $b = 1$, respectively.

C. Example 3

In this example, an asynchronous DS/CDMA channel for eight users ($K = 8$), each with three paths ($M_i = 3$, $i = 1, 2, \cdots, 8$) was considered. The users' spreading codes $c_j[n]$ are also Gold codes of length $\mathcal{P} = 31$. The channel parameters used were $A_{mk} = [\boldsymbol{A}]_{mk}$ and $\tau_{mk} = [\boldsymbol{T}]_{mk} T_c$, where

$$\boldsymbol{A}^T = \begin{bmatrix} 0.2 & -1.3 & -1.37 & 0.25 & 1.37 \\ -1.3 & 0.7 & -0.5 & -1.5 & -0.5 \\ 0.5 & -0.5 & -0.75 & -0.5 & 0.75 \\ -1.1 & 1.2 & 1.3 & & \\ 0.7 & -0.8 & 0.8 & & \\ -0.5 & 0.6 & 0.45 & & \end{bmatrix} \tag{45}$$

$$\boldsymbol{T}^T = \begin{bmatrix} 1.7 & 1.8 & 2.7 & 3.2 & 3.7 & 3.9 & 4.9 & 6.8 \\ 2.6 & 2.7 & 4.6 & 4.1 & 4.6 & 4.8 & 5.8 & 7.7 \\ 3.9 & 3.5 & 5.0 & 5.5 & 5.4 & 5.5 & 6.6 & 8.5 \end{bmatrix}. \tag{46}$$

The synthetic data $\mathbf{x}[n]$ for $N = 1500$, SNR $= 20$, 15, 10 dB, $\mathcal{M}_i = \tilde{\mathcal{M}} = 1$, and $\mathcal{M}_i = \tilde{\mathcal{M}} = 3$ for all i were processed by Algorithm 2 with $p = q = r = s = 2$. The length of equalizer $L = 8$ ($L_1 = 0$ and $L_2 = 7$) and $L = 4$ ($L_1 = 0$ and $L_2 = 3$) for $\tilde{\mathcal{M}} = 1$ and $\tilde{\mathcal{M}} = 3$, respectively. The initial conditions $\mathbf{v}^{(0)}[n]$ were chosen as (41) with $j = 2$ and $n_0 = 1$ and $n_0 = 3$ for $\tilde{\mathcal{M}} = 1$ and $\tilde{\mathcal{M}} = 3$, respectively, to initialize Algorithm 2 for estimating $u_2[n]$ (i.e., only user 2 is the desired user).

Simulation results for $\tilde{\mathcal{M}} = 1$ are shown in Fig. 7. Thirty optimum overall channel estimates $\hat{s}[n = 6(k-1) + m]$ (=

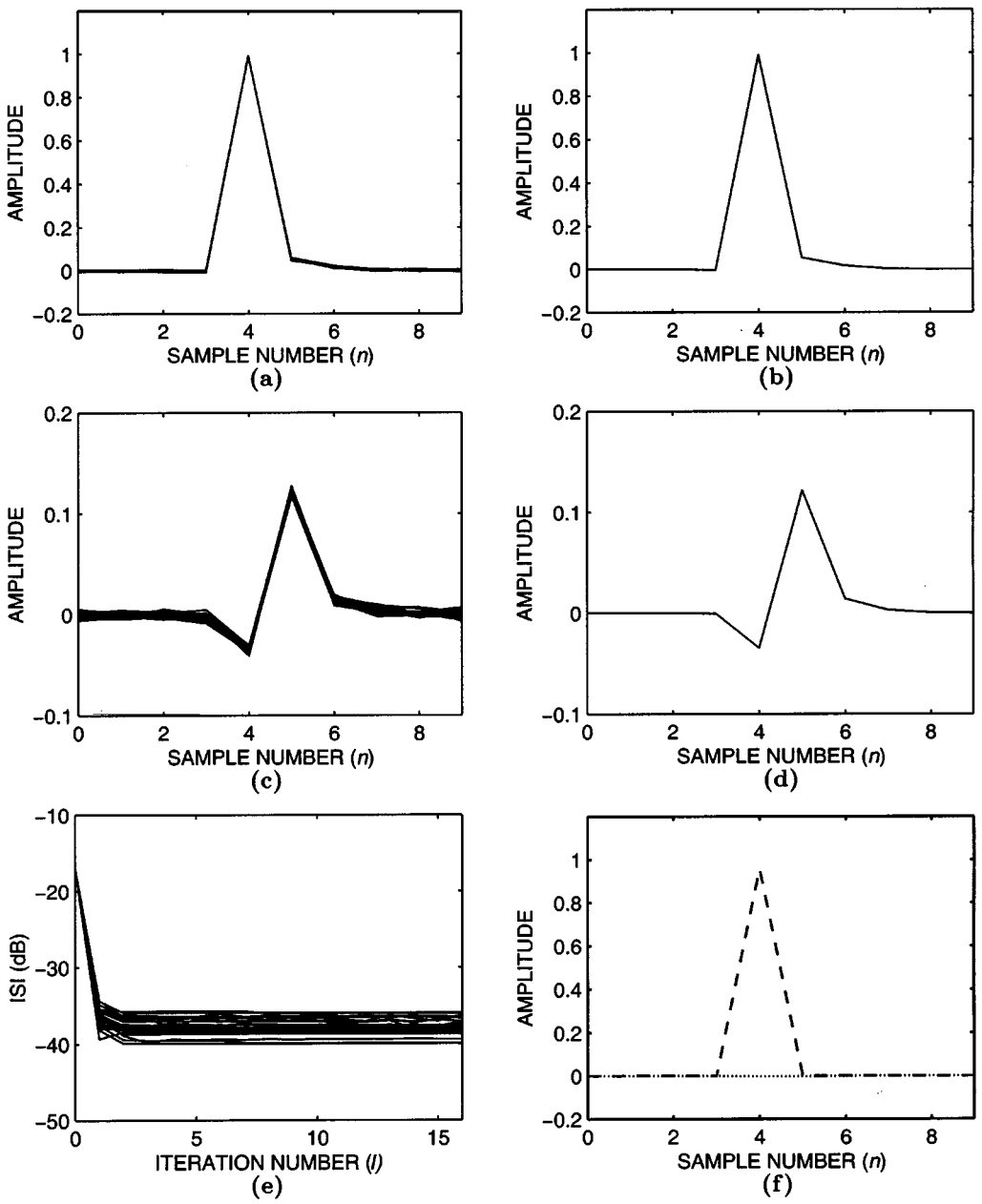

Fig. 5. Simulation results of Example 2 associated with $e[n] = \hat{u}_1[n]$. (a) Thirty $\hat{v}_1[n]$s and (c) $\hat{v}_2[n]$s obtained by Algorithm 2. (b) True $v_1[n]$ and (d) $v_2[n]$ obtained by Algorithm 1. (e) Associated 30 ISIs obtained by Algorithm 2. (f) Overall channel $s_1[n]$ (dash line) and $s_2[n]$ (dotted line) associated with the true $\mathbf{v}[n]$.

$s_k[m]$, $k = 1, 2, \cdots, 8$, $m = 0, 1, \cdots, 5$) are illustrated in Fig. 7(a), (c), and (e) for SNR = 20, 15, and 10 dB, respectively, and the associated ISIs are depicted in Fig. 7(b), (d), and (f), respectively. The corresponding results for $\tilde{\mathcal{M}} = 3$ are shown in Fig. 8(a)–(f), respectively. One can see, from these figures, that the overall channel impulse response $\mathbf{s}[n] \simeq \boldsymbol{\varepsilon}_2\delta[n-3]$ and $\mathbf{s}[n] \simeq \boldsymbol{\varepsilon}_2\delta[n-1]$ for $\tilde{\mathcal{M}} = 1$ and $\tilde{\mathcal{M}} = 3$, respectively, except for a scale factor implying that 30 estimates $e[n] = \hat{u}_2[n]$ were obtained and that all the ISIs converge fast (by spending two to four iterations) with the resultant ISIs smaller for larger SNR. Moreover, one can observe that results shown in Fig. 8(b), (d), and (f) are about 7 dB better than those shown in Fig. 7(b), (d), and (f), respectively, because multipath diversity ($\tilde{\mathcal{M}} = 3$) for the former is exploited. These simulation results support that Algorithm 2 works well for the MAI and ISI suppression of the eight-user asynchronous DS/CDMA system used in this example.

VI. Conclusions

We have presented three properties for the MIMO linear equalizer $\mathbf{v}[n]$ associated with Chi and Chen's MIMO-IFC for any SNR, including perfect phase equalization, a relation to the nonblind MIMO-MMSE equalizer, and the equivalence to the one associated with MIMO-SEA, as presented in Properties 1, 2, and 3, respectively. Based on Property 2, a fast iterative algorithm (Algorithm 1) was proposed for computing the true equalizer during the simulation stage, but it is never an MIMO

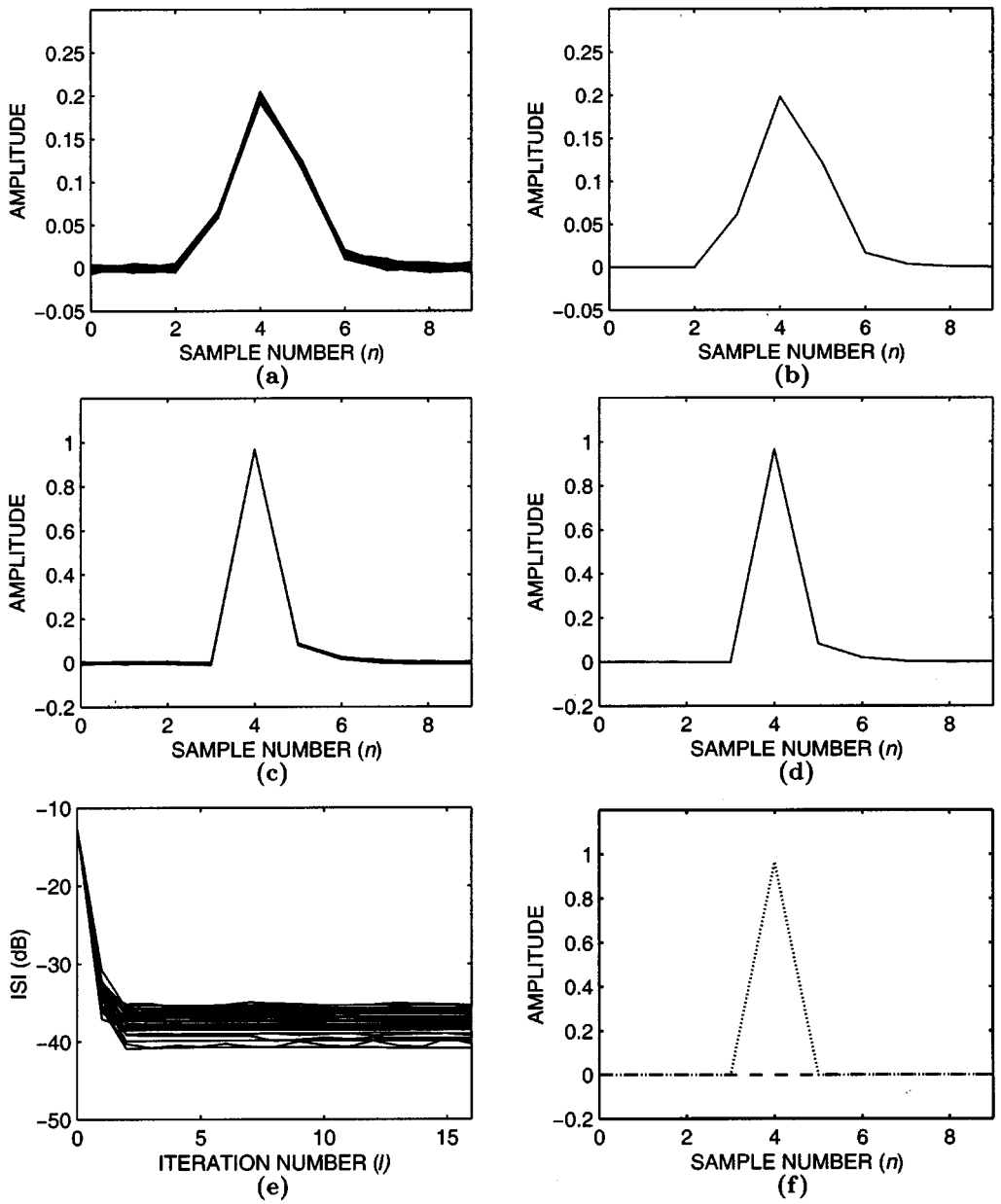

Fig. 6. Simulation results of Example 2 associated with $e[n] = \hat{u}_2[n]$. (a) Thirty $\hat{v}_1[n]$s and (c) $\hat{v}_2[n]$s obtained by Algorithm 2. (b) True $v_1[n]$ and (d) $v_2[n]$ obtained by Algorithm 1. (e) Associated 30 ISIs obtained by Algorithm 2. (f) Overall channel $s_1[n]$ (dash line) and $s_2[n]$ (dotted line) associated with the true $\mathbf{v}[n]$.

blind deconvolution algorithm for processing data. Based on Property 3, a fast MIMO-IFC based algorithm (Algorithm 2) was presented that performs as the MIMO-SEA (in terms of ISI, computational load, and convergence speed) with guaranteed convergence, whereas the latter may not converge for finite SNR and data. Then, the application of Algorithm 2 to MAI and ISI suppression for asynchronous DS/CDMA systems was presented. Some simulation results were also presented for supporting the proposed analytical results and Algorithm 2. The proposed analytic properties of MIMO-IFC are helpful to the behavior and implementation of the designed equalizer and the interpretation of the deconvolved signals. More studies of applying the proposed Algorithm 2 to multiuser communications and other statistical signal processing areas such as seismic deconvolution and source separation are left for future research.

APPENDIX A
PROOF OF PROPERTY 1

Because $[\mathbf{Q}[k]]_{il} = 0$ for $i \neq l$, it can be easily shown, from (6), that the noise variance $r_{ww}[0]$ is given by

$$r_{ww}[0] = \sum_{l=1}^{P} [\mathbf{Q}[k]]_{ll} * v_l[k] * v_l^*[-k]\Big|_{k=0}. \tag{A.1}$$

By (4), (7), (A.1), and Parseval's relation [36], $C_{1,1}\{c(n)\}$ can be

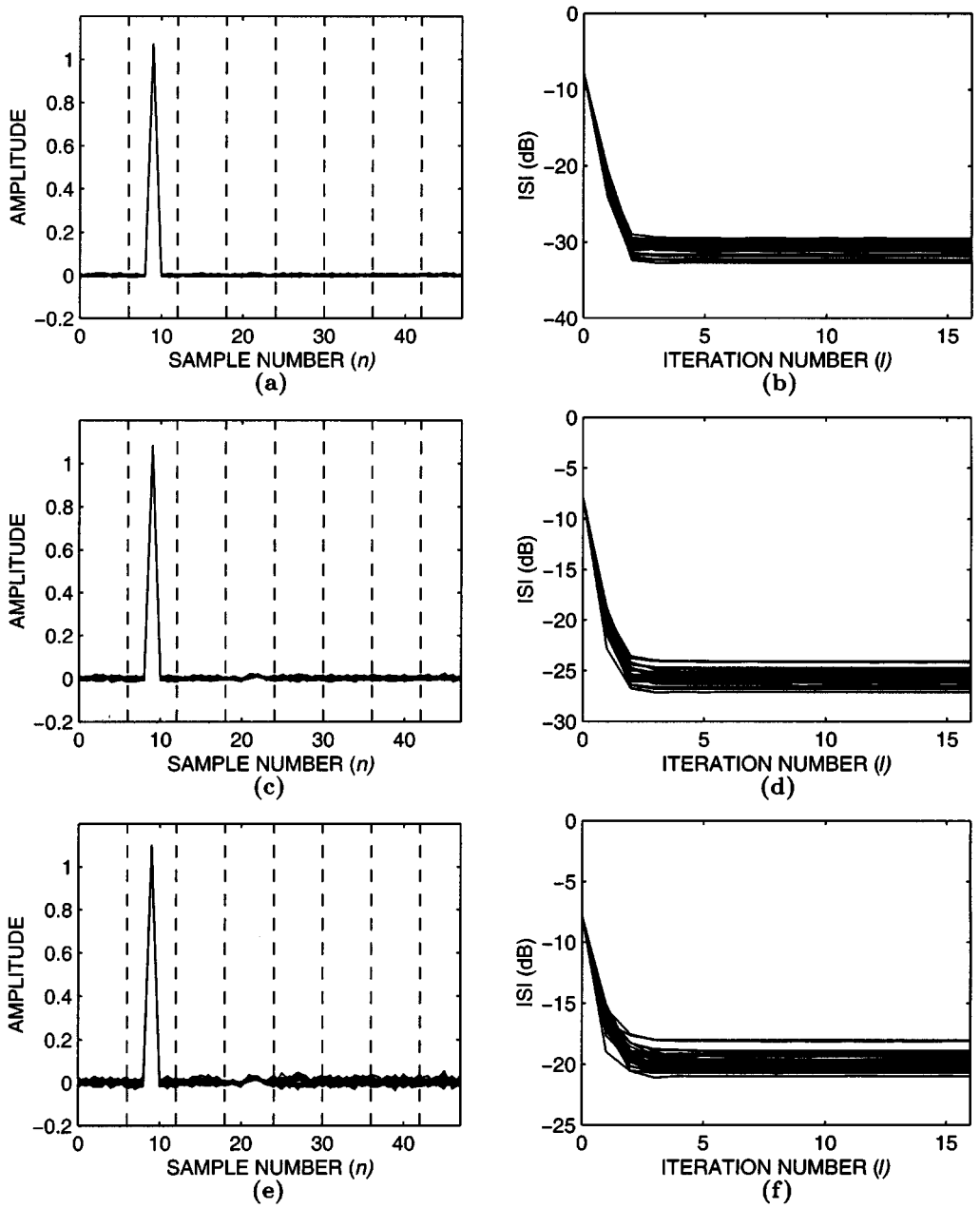

Fig. 7. Simulation results of Example 3 associated with $e[n] = \hat{u}_2[n]$ for $\bar{\mathcal{M}} = 1$. (a) and (b) Thirty optimum overall channel estimates $\hat{s}[n = 6(k-1)+m]$ $(= s_k[m],\ k = 1, 2, \cdots, 8,\ m = 0, 1, \cdots, 5)$ and associated ISIs, respectively, for SNR = 20 dB. (c) and (d) Thirty optimum overall channel estimates $\hat{s}[n]$ and associated ISIs, respectively, for SNR = 15 dB. (e) and (f) Thirty optimum overall channel estimates $\hat{s}[n]$ and associated ISIs, respectively, for SNR = 10 dB.

simplified as

$$C_{1,1}\{e(n)\} = \sum_{l=1}^{P}\sum_{k=1}^{K} C_{1,1}\{u_k[n]\} \cdot \left(\sum_{n=-\infty}^{\infty} |[\mathbf{H}[n]]_{lk} * v_l[n]|^2\right) + r_{ww}[0] \quad \text{(A.2)}$$

$$= \frac{1}{2\pi}\sum_{l=1}^{P}\int_{-\pi}^{\pi}\left[\left(\sum_{k=1}^{K} C_{1,1}\{u_k[n]\}\cdot|[\mathcal{H}(\omega)]_{lk}|^2\right) + |[\mathcal{Q}(\omega)]_{ll}|^2\right]\cdot|V_l(\omega)|^2\, d\omega \quad \text{(A.3)}$$

where

$$[\mathcal{H}(\omega)]_{lk} = \mathcal{F}\{[\mathbf{H}[n]]_{lk}\}$$
$$[\mathcal{Q}(\omega)]_{lk} = \mathcal{F}\{[\mathbf{Q}[n]]_{lk}\} \quad \text{and}$$
$$V_l(\omega) = \mathcal{F}\{v_l[n]\}.$$

One can see, from (A.3), that the denominator $|C_{1,1}\{e(n)\}|^{(p+q)/2}$ of $J_{p,q}(\boldsymbol{\nu})$ [see (10)] is dependent on $|V_l(\omega)|$ but independent of $\arg[V_l(\omega)]$.

Let

$$C_{p,q}\{u_k[n]\} = |C_{p,q}\{u_k[n]\}|\exp\{j\kappa_k\}$$
$$S_k(\omega) = \mathcal{F}\{s_k[n]\} = |S_k(\omega)|\exp\{j\Phi_k(\omega)\}$$

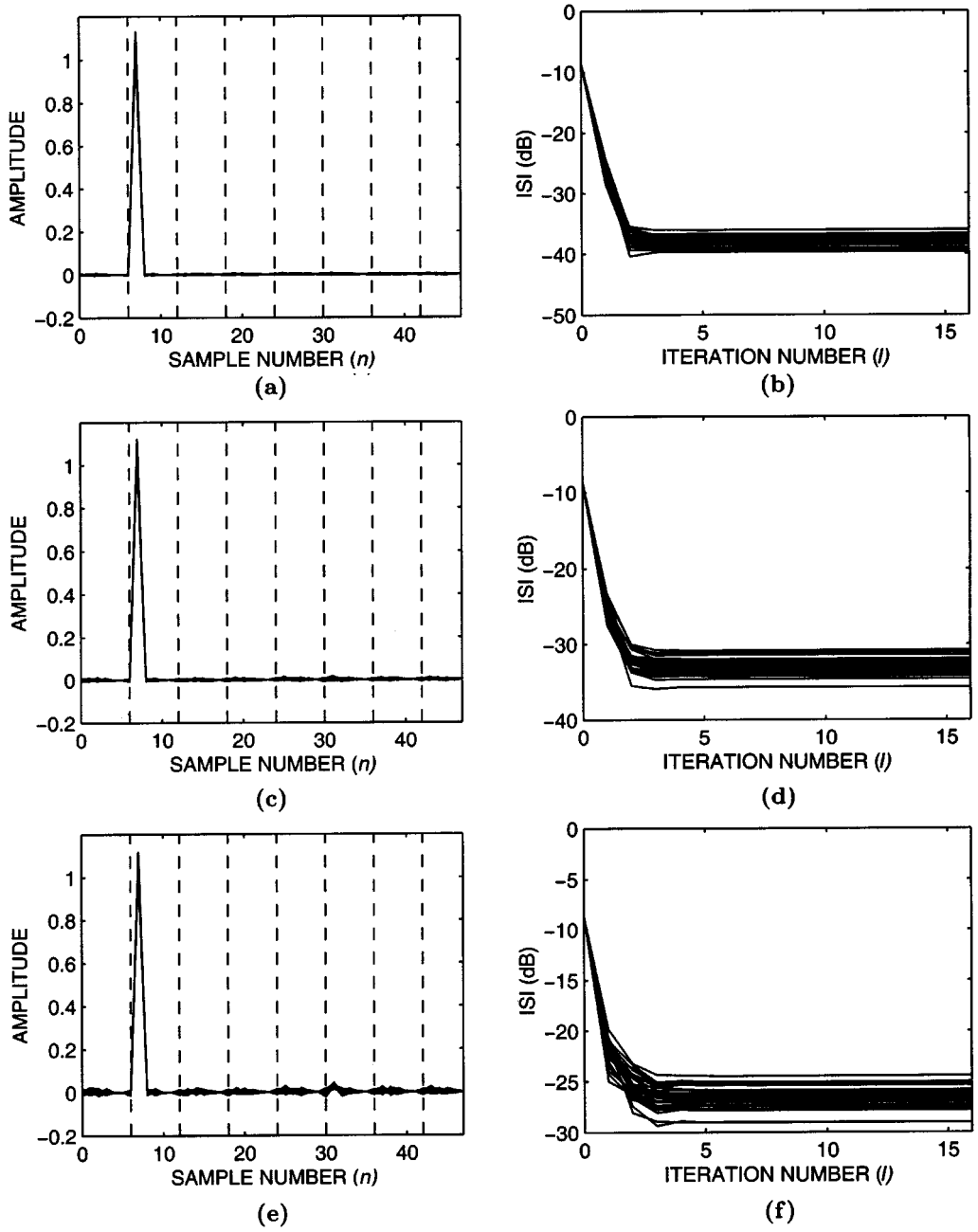

Fig. 8. Simulation results of Example 3 associated with $e[n] = \hat{u}_2[n]$ for $\bar{\mathcal{M}} = 3$. (a) and (b) Thirty optimum overall channel estimates $\hat{s}[n = 6(k-1)+m]$ $(= s_k[m],\ k = 1, 2, \cdots, 8,\ m = 0, 1, \cdots, 5)$ and associated ISIs, respectively, for SNR = 20 dB. (c) and (d) Thirty optimum overall channel estimates $\hat{s}[n]$ and associated ISIs, respectively, for SNR = 15 dB. (e) and (f) Thirty optimum overall channel estimates $\hat{s}[n]$ and associated ISIs, respectively, for SNR = 10 dB.

and let $C^{e}_{p,q}(\tau_1, \cdots, \tau_{p+q-1})$ denote the $(p+q)$th-order cumulant function of $e[n]$ defined as

$$C^{e}_{p,q}(\tau_1, \cdots, \tau_{p+q-1}) = \text{cum}\{e[n], e[n+\tau_1], \cdots, e[n+\tau_{p-1}] \; e^*[n-\tau_p], \cdots, e^*[n-\tau_{p+q-1}]\} \tag{A.4}$$

whose $(p+q-1)$-dimensional Fourier transform, which is denoted $\mathcal{S}^{e}_{p,q}(\omega_1, \cdots, \omega_{p+q-1})$ and known as the $(p+q)$th-order polyspectrum of $e[n]$ [5], can be shown to be [37]

$$\mathcal{S}^{e}_{p,q}(\omega_1, \cdots, \omega_{p+q-1}) = \sum_{k=1}^{K} C_{p,q}\{u_k[n]\} \cdot S_k\left(-\sum_{i=1}^{p-1}\omega_i + \sum_{i=p}^{p+q-1}\omega_i\right) \cdot \prod_{i=1}^{p-1} S_k(\omega_i) \cdot \prod_{i=p}^{p+q-1} S_k^*(\omega_i). \tag{A.5}$$

By (A.5), the numerator of $J_{p,q}(\boldsymbol{\nu})$ [see (10)] can be shown to

be

$$
\begin{aligned}
|C_{p,q}\{e[n]\}| &= |C^{e}_{p,q}(\tau_1=0,\tau_2=0,\cdots,\tau_{p+q-1}=0)| \\
&= \left|\left(\frac{1}{2\pi}\right)^{p+q-1}\int_{-\pi}^{\pi}\cdots\int_{-\pi}^{\pi} \right. \\
&\quad \left. \cdot\mathcal{S}^{e}_{p,q}(\omega_1,\cdots,\omega_{p+q-1})\,d\omega_1\cdots d\omega_{p+q-1}\right| \\
&= \left|\left(\frac{1}{2\pi}\right)^{p+q-1}\sum_{k=1}^{K}|C_{p,q}\{u_k[n]\}|\cdot\int_{-\pi}^{\pi}\cdots\int_{-\pi}^{\pi}\right. \\
&\quad \cdot\left|S_k\left(-\sum_{i=1}^{p-1}\omega_i+\sum_{i=p}^{p+q-1}\omega_i\right)\right|\cdot\prod_{i=1}^{p+q-1}|S_k(\omega_i)| \\
&\quad \cdot\exp\left\{j\left[\Phi_k\left(-\sum_{i=1}^{p-1}\omega_i+\sum_{i=p}^{p+q-1}\omega_i\right)\right.\right. \\
&\quad \left.\left.+\sum_{i=1}^{p-1}\Phi_k(\omega_i)-\sum_{i=p}^{p+q-1}\Phi_k(\omega_i)+\kappa_k\right]\right\} \\
&\quad \left. d\omega_1\cdots d\omega_{p+q-1}\right| \\
&\le \left(\frac{1}{2\pi}\right)^{p+q-1}\sum_{k=1}^{K}|C_{p,q}\{u_k[n]\}|\cdot\int_{-\pi}^{\pi}\cdots\int_{-\pi}^{\pi} \\
&\quad \cdot\left|S_k\left(-\sum_{i=1}^{p-1}\omega_i+\sum_{i=p}^{p+q-1}\omega_i\right)\right| \\
&\quad \cdot\prod_{i=1}^{p+q-1}|S_k(\omega_i)|\,d\omega_1\cdots d\omega_{p+q-1}. \qquad \text{(A.6)}
\end{aligned}
$$

One can easily see that the equality of (A.6) requires

$$
\begin{aligned}
&\Phi_k\left(-\sum_{i=1}^{p-1}\omega_i+\sum_{i=p}^{p+q-1}\omega_i\right)+\sum_{i=1}^{p-1}\Phi_k(\omega_i) \\
&\quad -\sum_{i=p}^{p+q-1}\Phi_k(\omega_i)+\kappa_k=\varphi, \\
&\quad \forall\omega\in[-\pi,\pi), \qquad k=1,\cdots,K \qquad \text{(A.7)}
\end{aligned}
$$

where φ is a constant independent of ω. Therefore, the optimum $\Phi_k(\omega)$ associated with the maximum of $J_{p,q}(\boldsymbol{\nu})$ is linear for $\omega\in[-\pi,\pi)$, i.e., the optimum $\Phi_k(\omega)=\arg[S_k(\omega)]$ can be expressed as (17), regardless of $|V_l(\omega)|$, $l=1,2,\cdots,P$.

Appendix B
Proof of Lemma 1

The joint cumulant of l random variables y_i, $i=1,2,\cdots,l$ can be expressed as [5]

$$
\begin{aligned}
&\text{cum}\{y_1,y_2,\cdots,y_l\} \\
&\quad=\sum_{t=1}^{l}(-1)^{t-1}[(t-1)!]\cdot E\left[\prod_{i\in\Omega_1}y_i\right] \\
&\qquad\cdot E\left[\prod_{i\in\Omega_2}y_i\right]\cdots E\left[\prod_{i\in\Omega_t}y_i\right] \qquad \text{(B.1)}
\end{aligned}
$$

where the summation includes all possible partitions $\{\Omega_1,\Omega_2,\cdots,\Omega_t\}$ of the integer set $\mathbf{I}=\{1,2,\cdots,l\}$. By (B.1), we obtain

$$
\begin{aligned}
C_{p,q}\{e[n]\} &= \text{cum}\{e[n]:p,e^*[n]:q\} \\
&= \sum_{t=1}^{p+q}(-1)^{t-1}[(t-1)!] \\
&\quad\cdot\prod_{k=1}^{p+q}E[e^{i_k}[n](e^*[n])^{j_k}] \qquad \text{(B.2)}
\end{aligned}
$$

where i_k and j_k are numbers of terms of $e[n]$ and $e^*[n]$ in the associated partition of Ω_k, satisfying $\sum_{k=1}^{p+q}i_k=p$ and $\sum_{k=1}^{p+q}j_k=q$, respectively. It can be easily seen from (B.2) that

$$
\begin{aligned}
C^{*}_{p,q}\{e[n]\} &= \sum_{t=1}^{p+q}(-1)^{t-1}[(t-1)!] \\
&\quad\cdot\prod_{k=1}^{p+q}E[(e^*[n])^{i_k}e^{j_k}[n]]=C_{q,p}\{e[n]\} \qquad \text{(B.3)}
\end{aligned}
$$

which is equivalent to (23). Next, let us prove (24).

It is easy to see from (2) that

$$
\frac{\partial e[n]}{\partial\boldsymbol{\nu}^*}=\mathbf{0} \qquad \text{(B.4)}
$$

$$
\frac{\partial e^*[n]}{\partial\boldsymbol{\nu}^*}=\tilde{\boldsymbol{x}}^*[n]. \qquad \text{(B.5)}
$$

Taking the partial derivative of $C_{p,q}\{e[n]\}$ given by (B.2) with respect to $\boldsymbol{\nu}^*$ yields

$$
\begin{aligned}
\frac{\partial C_{p,q}\{e[n]\}}{\partial\boldsymbol{\nu}^*} &= \sum_{t=1}^{p+q}(-1)^{t-1}[(t-1)!] \\
&\quad\cdot\left\{\sum_{m=1}^{p+q}j_m\cdot\left(\prod_{k=1,k\neq m}^{p+q}E[e^{i_k}[n](e^*[n])^{j_k}]\right)\right. \\
&\quad\left.\cdot E[e^{i_m}[n](e^*[n])^{j_m-1}\tilde{\boldsymbol{x}}^*[n]]\right\} \\
&\quad\text{[by (B.4) and (B.5)]} \\
&= \sum_{m=1}^{p+q}j_m\cdot\left\{\sum_{t=1}^{p+q}(-1)^{t-1}[(t-1)!]\right. \\
&\quad\cdot\left[\left(\prod_{k=1,k\neq m}^{p+q}E[e^{i_k}[n](e^*[n])^{j_k}]\right)\right. \\
&\quad\left.\left.\cdot E[e^{i_m}[n](e^*[n])^{j_m-1}\tilde{\boldsymbol{x}}^*[n]]\right]\right\} \\
&= \left(\sum_{m=1}^{p+q}j_m\right)\cdot\text{cum}\{e[n]:p,e^*[n]:q-1,\tilde{\boldsymbol{x}}^*[n]\} \\
&\quad\text{[by (B.2)]} \\
&= q\cdot\text{cum}\{e[n]:p,e^*[n]:q-1,\tilde{\boldsymbol{x}}^*[n]\} \qquad \text{(B.6)}
\end{aligned}
$$

which is (24). Thus, we have completed the proof.

APPENDIX C
PROOF OF PROPERTY 2

First of all, let us prove that $\partial C_{1,1}\{e[n]\}/\partial \boldsymbol{\nu}^*$ and $\text{cum}\{e[n] : p, e^*[n] : q-1, (x_i[n-k])^*\}$ can be expressed as (C.1) and (C.2), respectively, for ease of use in the Proof of Property 2 below. By (24), we have

$$\frac{\partial C_{1,1}\{e[n]\}}{\partial \boldsymbol{\nu}^*} = E[e[n]\tilde{\boldsymbol{x}}^*[n]] = E[\tilde{\boldsymbol{x}}^*[n]\tilde{\boldsymbol{x}}^T[n]\boldsymbol{\nu}] = \tilde{\boldsymbol{R}}\boldsymbol{\nu} \tag{C.1}$$

where $\tilde{\boldsymbol{R}} = E[\tilde{\boldsymbol{x}}^*[n]\tilde{\boldsymbol{x}}^T[n]]$ was defined at the beginning of Section II. On the other hand

$$\begin{aligned}
&\text{cum}\{e[n] : p, e^*[n] : q-1, (x_i[n-k])^*\} \\
&\quad = \text{cum}\left\{\sum_{l=1}^{K}\sum_{k_1=-\infty}^{\infty} s_l[n-k_1]u_l[k_1] : p \right. \\
&\qquad \sum_{l=1}^{K}\sum_{k_1=-\infty}^{\infty} s_l^*[n-k_1]u_l^*[k_1] : q-1 \\
&\qquad \left. \sum_{l=1}^{K}\sum_{k_1=-\infty}^{\infty} [\mathbf{H}[n-k_1-k]]_{il}^* u_l^*[k_1]\right\} \quad \text{[by (3)]} \\
&\quad = \sum_{l=1}^{K} C_{p,q}\{u_l[n]\} \sum_{k_1=-\infty}^{\infty} s_l^p[k_1](s_l^*[k_1])^{q-1} \\
&\qquad \cdot [\mathbf{H}[k_1-k]]_{il}^* \quad \text{[by } (\mathcal{A}1)\text{]} \\
&\quad = \sum_{l=1}^{K} C_{p,q}\{u_l[n]\} \cdot (g_{pql}[k] * [\mathbf{H}[-k]]_{il}^*) \\
&\qquad i = 1, \cdots, P, \quad k = L_1, \cdots, L_2
\end{aligned} \tag{C.2}$$

where $g_{pql}[k]$ was defined by (18).

Maximizing $J_{p,q}(\boldsymbol{\nu})$ given by (10) is equivalent to maximizing

$$\begin{aligned}
\tilde{J}_{p,q}(\boldsymbol{\nu}) = J_{p,q}^2(\boldsymbol{\nu}) &= \frac{|C_{p,q}\{e[n]\}|^2}{|C_{1,1}\{e[n]\}|^{p+q}} \\
&= \frac{C_{p,q}\{e[n]\}C_{q,p}\{e[n]\}}{|C_{1,1}\{e[n]\}|^{p+q}} \quad \text{[by (23)]}
\end{aligned} \tag{C.3}$$

which implies

$$\frac{\partial \tilde{J}_{p,q}(\boldsymbol{\nu})}{\partial \boldsymbol{\nu}^*} = 2 \cdot J_{p,q}(\boldsymbol{\nu}) \cdot \frac{\partial J_{p,q}(\boldsymbol{\nu})}{\partial \boldsymbol{\nu}^*}. \tag{C.4}$$

Taking partial derivative of $\tilde{J}_{p,q}(\boldsymbol{\nu})$ given by (C.3) with respect to $\boldsymbol{\nu}^*$ yields

$$\begin{aligned}
\frac{\partial \tilde{J}_{p,q}}{\partial \boldsymbol{\nu}^*} = \tilde{J}_{p,q} \cdot \Bigg\{ &\frac{1}{C_{q,p}\{e[n]\}} \cdot \frac{\partial C_{q,p}\{e[n]\}}{\partial \boldsymbol{\nu}^*} \\
&+ \frac{1}{C_{p,q}\{e[n]\}} \cdot \frac{\partial C_{p,q}\{e[n]\}}{\partial \boldsymbol{\nu}^*} \\
&- \frac{p+q}{C_{1,1}\{e[n]\}} \cdot \frac{\partial C_{1,1}\{e[n]\}}{\partial \boldsymbol{\nu}^*} \Bigg\}
\end{aligned} \tag{C.5}$$

which together with (C.4) leads to

$$\begin{aligned}
\frac{\partial J_{p,q}}{\partial \boldsymbol{\nu}^*} = \frac{J_{p,q}}{2} \cdot \Bigg\{ &\frac{1}{C_{q,p}\{e[n]\}} \cdot \frac{\partial C_{q,p}\{e[n]\}}{\partial \boldsymbol{\nu}^*} \\
&+ \frac{1}{C_{p,q}\{e[n]\}} \cdot \frac{\partial C_{p,q}\{e[n]\}}{\partial \boldsymbol{\nu}^*} - \frac{p+q}{C_{1,1}\{e[n]\}} \\
&\cdot \frac{\partial C_{1,1}\{e[n]\}}{\partial \boldsymbol{\nu}^*} \Bigg\}.
\end{aligned} \tag{C.6}$$

Setting $\partial J_{p,q}/\partial \boldsymbol{\nu}^*$ given by (C.6) equal to zero and substituting (C.1) and (24) into the resultant equation, we obtain

$$\begin{aligned}
\tilde{\boldsymbol{R}}\boldsymbol{\nu} &= \frac{C_{1,1}\{e[n]\}}{p+q} \cdot \frac{p}{C_{q,p}\{e[n]\}} \\
&\quad \cdot \text{cum}\{e[n] : q, e^*[n] : p-1, \tilde{\boldsymbol{x}}^*[n]\} \\
&\quad + \frac{C_{1,1}\{e[n]\}}{p+q} \cdot \frac{q}{C_{p,q}\{e[n]\}} \\
&\quad \cdot \text{cum}\{e[n] : p, e^*[n] : q-1, \tilde{\boldsymbol{x}}^*[n]\} \\
&= \alpha_{q,p} \cdot \text{cum}\{e[n] : q, e^*[n] : p-1, \tilde{\boldsymbol{x}}^*[n]\} \\
&\quad + \alpha_{p,q} \cdot \text{cum}\{e[n] : p, e^*[n] : q-1, \tilde{\boldsymbol{x}}^*[n]\}
\end{aligned} \tag{C.7}$$

where $\alpha_{p,q}$ was defined by (22). Then, substituting (C.2) in (C.7), one can obtain

$$\begin{aligned}
&\sum_{l=1}^{P}\sum_{k=L_1}^{L_2} r_{i,l}^*[k-n]v_l[k] \\
&\quad = \sum_{l=1}^{P} r_{l,i}[n] * v_l[n] \\
&\quad = \alpha_{q,p} \cdot \sum_{l=1}^{K} C_{q,p}\{u_l[n]\} \cdot [g_{qpl}[n] * [\mathbf{H}[-n]]_{il}^*] \\
&\qquad + \alpha_{p,q} \cdot \sum_{l=1}^{K} C_{p,q}\{u_l[n]\} \cdot [g_{pql}[n] * [\mathbf{H}[-n]]_{il}^*] \\
&\qquad i = 1, \cdots, P, \quad n = L_1, \cdots, L_2
\end{aligned} \tag{C.8}$$

where

$$r_{i,l}[k] = E[x_i[n]x_l^*[n-k]] = r_{l,i}^*[-k].$$

Let $L_1 \to -\infty$ and $L_2 \to \infty$, and then, taking the discrete-time Fourier transform of both sides of (C.8) yields

$$\begin{aligned}
\mathcal{R}^T(\omega)\boldsymbol{V}(\omega) = &\alpha_{q,p}\mathcal{H}^*(\omega)\mathbf{D}_{q,p}\boldsymbol{G}_{q,p}(\omega) \\
&+ \alpha_{p,q}\mathcal{H}^*(\omega)\mathbf{D}_{p,q}\boldsymbol{G}_{p,q}(\omega)
\end{aligned} \tag{C.9}$$

where $\mathbf{D}_{p,q}$, $\mathcal{R}(\omega)$, and $\boldsymbol{G}_{p,q}(\omega)$ were defined by (14), (16), and (19), respectively. Finally, from (C.9) and (15), we obtain

$$\begin{aligned}
\boldsymbol{V}(\omega) &= [\mathcal{R}^T(\omega)]^{-1} \cdot \mathcal{H}^*(\omega)(\alpha_{q,p}\mathbf{D}_{q,p}\boldsymbol{G}_{q,p}(\omega) \\
&\qquad + \alpha_{p,q}\mathbf{D}_{p,q}\boldsymbol{G}_{p,q}(\omega)) \\
&= \mathcal{V}_{\text{MMSE}}^T(\omega) \cdot \mathbf{D}_{1,1}^{-1} \cdot (\alpha_{q,p}\mathbf{D}_{q,p}\boldsymbol{G}_{q,p}(\omega) \\
&\qquad + \alpha_{p,q}\mathbf{D}_{p,q}\boldsymbol{G}_{p,q}(\omega)) \\
&= \mathcal{V}_{\text{MMSE}}^T(\omega) \cdot \tilde{\boldsymbol{G}}(\omega)
\end{aligned} \tag{C.10}$$

where $\mathbf{D}_{p,q}$ and $\tilde{\boldsymbol{G}}(\omega)$ were defined by (14) and (21), respectively. Thus, we have completed the proof.

APPENDIX D
PROOF OF PROPERTY 3

As $\mathbf{x}[n]$ is complex, letting $p=q$ in (C.7) yields

$$\tilde{\boldsymbol{R}}\boldsymbol{\nu} = 2\cdot\alpha_{p,p}\cdot\text{cum}\{e[n]:p,e^*[n]:p-1,\tilde{\boldsymbol{x}}^*[n]\} \quad \text{(D.1)}$$

which is equivalent to (11) with $r=s=p=q$, except for a scale factor. Similarly, as $\mathbf{x}[n]$ is real, and one can also obtain from (C.7) that

$$\begin{aligned}\tilde{\boldsymbol{R}}\boldsymbol{\nu} &= (\alpha_{p,q}+\alpha_{q,p})\cdot\text{cum}\{e[n]:p+q-1,\tilde{\boldsymbol{x}}[n]\}\\ &= \frac{C_{1,1}\{e[n]\}}{C_{p,q}\{e[n]\}}\cdot\text{cum}\{e[n]:p+q-1,\tilde{\boldsymbol{x}}[n]\} \quad \text{(D.2)}\end{aligned}$$

which is also equivalent to (11) with $r+s=p+q$, except for a scale factor. Thus we have completed the proof.

APPENDIX E
PROOF OF (26)

It can be easily shown from (C.6), (C.1), and (24) that

$$\begin{aligned}\frac{\partial J_{p,q}(\boldsymbol{\nu})}{\partial\boldsymbol{\nu}^*} = \frac{J_{p,q}}{2}\cdot\Bigg\{&\frac{p}{C_{q,p}\{e[n]\}}\\ &\cdot\text{cum}\{e[n]:q,e^*[n]:p-1,\tilde{\boldsymbol{x}}^*[n]\}\\ &+\frac{q}{C_{p,q}\{e[n]\}}\cdot\text{cum}\{e[n]:p,e^*[n]:q-1,\tilde{\boldsymbol{x}}^*[n]\}\\ &-\frac{p+q}{C_{1,1}\{e[n]\}}\cdot\tilde{\boldsymbol{R}}\boldsymbol{\nu}\Bigg\}. \quad \text{(E.1)}\end{aligned}$$

As $\mathbf{x}[n]$ is complex and $p=q=r=s$, it can be obtained from (E.1) that

$$\frac{\partial J_{p,p}(\boldsymbol{\nu})}{\partial\boldsymbol{\nu}^*} = p\cdot J_{p,p}\cdot\left(\frac{1}{C_{p,p}\{e[n]\}}\cdot\tilde{\boldsymbol{d}}-\frac{1}{C_{1,1}\{e[n]\}}\cdot\tilde{\boldsymbol{R}}\boldsymbol{\nu}\right). \quad \text{(E.2)}$$

Again, one can easily show from (C.6) and (E.2), that

$$\begin{aligned}\frac{\partial J_{p,p}(\boldsymbol{\nu})}{\partial\boldsymbol{\nu}} = \left(\frac{\partial J_{p,p}(\boldsymbol{\nu})}{\partial\boldsymbol{\nu}^*}\right)^* &= p\cdot J_{p,p}\\ &\cdot\left(\frac{1}{C_{p,p}\{e[n]\}}\cdot\tilde{\boldsymbol{d}}^*-\frac{1}{C_{1,1}\{e[n]\}}\cdot(\tilde{\boldsymbol{R}}\boldsymbol{\nu})^*\right) \quad \text{(E.3)}\end{aligned}$$

which leads to (26) with $e[n]$, $\tilde{\boldsymbol{d}}$, and $\boldsymbol{\nu}$ replaced by $e^{(I-1)}[n]$, $\tilde{\boldsymbol{d}}^{(I-1)}$, and $\boldsymbol{\nu}_{I-1}$, respectively.

As $\mathbf{x}[n]$ is real (i.e., $\boldsymbol{\nu}$, $\tilde{\boldsymbol{d}}$ and $\tilde{\boldsymbol{R}}$ are real) and $p+q=r+s$, it can be seen from (E.1) that

$$\begin{aligned}\frac{\partial J_{p,q}(\boldsymbol{\nu})}{\partial\boldsymbol{\nu}} = \frac{\partial J_{p,q}(\boldsymbol{\nu})}{\partial\boldsymbol{\nu}^*} &= \frac{(p+q)\cdot J_{p,q}}{2}\\ &\cdot\left(\frac{1}{C_{p,q}\{e[n]\}}\cdot\text{cum}\{e[n]:p+q-1,\tilde{\boldsymbol{x}}[n]\}\right.\\ &\left.-\frac{1}{C_{1,1}\{e[n]\}}\cdot\tilde{\boldsymbol{R}}\boldsymbol{\nu}\right)\\ &= \frac{(p+q)\cdot J_{p,q}}{2}\\ &\cdot\left(\frac{1}{C_{p,q}\{e[n]\}}\cdot\tilde{\boldsymbol{d}}-\frac{1}{C_{1,1}\{e[n]\}}\cdot\tilde{\boldsymbol{R}}\boldsymbol{\nu}\right) \quad \text{(E.4)}\end{aligned}$$

which also leads to (26) with $e[n]$, $\tilde{\boldsymbol{d}}$, and $\boldsymbol{\nu}$ replaced by $e^{(I-1)}[n]$, $\tilde{\boldsymbol{d}}^{(I-1)}$ and $\boldsymbol{\nu}_{I-1}$, respectively. Thus, we have completed the proof.

REFERENCES

[1] S. Verdu, *Multiuser Detection*. Cambridge, U.K.: Cambridge Univ. Press, 1998.

[2] H. V. Poor and G. W. Wornell, *Wireless Communications: Signal Processing Perspective*. Englewood Cliffs, NJ: Prentice-Hall, 1998.

[3] H. Liu, *Signal Processing Applications in CDMA Communications*. Norwell, MA: Artech House, 2000.

[4] A. J. Paulraj and C. B. Padadias, "Space-time processing for wireless communications," *IEEE Signal Processing Mag.*, vol. 14, pp. 49–83, Nov. 1997.

[5] C. L. Nikias and A. P. Petropulu, *Higher-Order Spectra Analysis: A Nonlinear Signal Processing Framework*. Englewood Cliffs, NJ: Prentice-Hall, 1993.

[6] C.-Y. Chi and M.-C. Wu, "Inverse filter criteria for blind deconvolution and equalization using two cumulants," *Signal Process.*, vol. 43, no. 1, pp. 55–63, Apr. 1995.

[7] R. A. Wiggins, "Minimum entropy deconvolution," *Geoexploration*, vol. 16, pp. 21–35, 1978.

[8] O. Shalvi and E. Weinstein, "New criteria for blind deconvolution of nonminimum-phase systems (channels)," *IEEE Trans. Inform. Theory*, vol. 36, pp. 312–321, Mar. 1990.

[9] J. K. Tugnait, "Estimation of liner parametric models using inverse filter criteria and higher-order statistics," *IEEE Trans. Signal Processing*, vol. 41, pp. 3196–3199, Nov. 1993.

[10] O. Shalvi and E. Weinstein, "Universal methods for blind deconvolution," in *Blind Deconvolution*, S. Haykin, Ed. Englewood Cliffs, NJ: Prentice-Hall, 1994.

[11] C.-C. Feng and C.-Y. Chi, "Performance of cumulant based inverse filters for blind deconvolution," *IEEE Trans. Signal Processing*, vol. 47, pp. 1922–1935, July 1999.

[12] ——, "Performance of Shalvi and Weinstein's deconvolution criteria for channels with/without zeros on the unit circle," *IEEE Trans. Signal Processing*, vol. 48, pp. 571–575, Feb. 2000.

[13] O. Shalvi and E. Weinstein, "Super-exponential methods for blind deconvolution," *IEEE Trans. Inform. Theory*, vol. 39, pp. 504–519, Mar. 1993.

[14] C.-Y. Chi, C.-Y. Chen, and B.-W. Li, "On super-exponential algorithm, constant modulus algorithm and inverse filter criteria for blind equalization," in *Proc. IEEE SP Workshop Statist. Signal Array Processing*, Pocono Manor, PA, Aug. 14–16, 2000, pp. 216–220.

[15] J. R. Treichler and B. G. Agee, "A new approach to multipath correction of constant modulus signals," *IEEE Trans. Acoust., Speech, Signal Processing*, vol. ASSP-31, pp. 349–472, Apr. 1983.

[16] J. K. Tugnait, "Identification and deconvolution of multichannel linear nongaussian processes using higher-order statistics and inverse filter criteria," *IEEE Trans. Signal Processing*, vol. 45, pp. 658–672, Mar. 1997.

[17] ——, "Adaptive blind separation of convolutive mixtures of independent linear signals," *Signal Process.*, vol. 73, no. 1–2, pp. 139–152, Feb. 1999.

[18] C.-Y. Chi and C.-H. Chen, "Blind MAI and ISI suppression for DS/CDMA systems using HOS based inverse filter criteria," *IEEE Trans. Signal Processing*, to be published.

[19] Y. Inouye and T. Habe, "Multichannel blind equalization using second- and fourth-order cumulants," in *Proc. IEEE Signal Process. Workshop Higher Order Statist.*, Begur, Spain, 1995, pp. 96–100.

[20] Y. Inouye and T. Sato, "Iterative algorithms based on multistage criteria for multichannel blind deconvolution," *IEEE Trans. Signal Processing*, vol. 47, pp. 1759–1764, June 1999.

[21] Y. Inouye, "Criteria for blind deconvolution of multichannel linear time-invariant systems," *IEEE Trans. Signal Processing*, vol. 46, pp. 3432–3436, Dec. 1998.

[22] K. L. Yeung and S. F. Yau, "A cumulant-based super-exponential algorithm for blind deconvolution of multi-input multi-output systems," *Signal Process.*, vol. 67, no. 2, pp. 141–162, 1998.

[23] Y. Inouye and K. Tanebe, "Super-exponential algorithms for multichannel blind deconvolution," *IEEE Trans. Signal Processing*, vol. 48, pp. 881–888, Mar. 2000.

[24] J. Gomes and V. Barroso, "A super-exponential algorithm for blind fractionally spaced equalization," *IEEE Signal Processing Lett.*, vol. 3, pp. 283–285, Oct. 1996.
[25] Y. Li and K. J. R. Liu, "Adaptive source separation and equalization for multiple-input/multiple-output systems," *IEEE Trans. Inform. Theory*, vol. 44, pp. 2864–2876, Nov. 1998.
[26] C. B. Papadias and A. J. Paulraj, "A constant modulus algorithm for multiuser signal separation in presence of delay spread using antenna arrays," *IEEE Signal Processing Lett.*, vol. 4, pp. 178–181, June 1997.
[27] Y. Li and Z. Ding, "Global convergence of fractionally spaced Godard (CMA) adaptive equalizers," *IEEE Trans. Signal Processing*, vol. 44, pp. 818–826, Apr. 1996.
[28] Z. Ding and T. Nguyen, "Stationary points of a Kurtosis maximization algorithm for blind signal separation and antenna beamforming," *IEEE Trans. Signal Processing*, vol. 48, pp. 1587–1596, June 2000.
[29] D. M. Burley, *Studies in Optimization*. New York: Falsted–Wiley, 1974.
[30] C. W. Therrien, *Discrete-Time Random Signals and Statistical Signal Processing*. Englewood Cliffs, NJ: Prentice-Hall, 1992.
[31] G. Leus, "Signal processing algorithms for CDMA-based wireless communications," Ph.D. dissertation, Faculty of Applied Sciences, Katholiecke Univ. Leuven, Leuven, Belgium, May 2000.
[32] M. K. Tsatsanis and G. B. Giannakis, "Optimal decorrelating receivers for DS/CDMA systems: A signal processing framework," *IEEE Trans. Signal Processing*, vol. 44, pp. 3044–3055, Dec. 1996.
[33] M. K. Tsatsanis, "Inverse filtering criteria for CDMA systems," *IEEE Trans. Signal Processing*, vol. 45, pp. 102–112, Jan. 1997.
[34] M. K. Tsatsanis and Z. Xu, "Performance analysis of minimum variance CDMA receivers," *IEEE Trans. Signal Processing*, vol. 46, pp. 3014–3022, Nov. 1998.
[35] X. Wang and H. V. Poor, "Space-time processing in multiple-access systems," in *Proc. IEEE Wireless Commun. Networking Conf.*, New Orleans, LA, Sept. 21–24, 1999, pp. 129–133.
[36] A. V. Oppenheim and R. W. Schafer, *Discrete-Time Signal Processing*. Englewood Cliffs, NJ: Prentice-Hall, 1989.
[37] P. O. Amblard, M. Gaeta, and J. L. Lacoume, "Statistics for complex variables and signals—Part II: Signals," *Signal Process.*, vol. 53, pp. 15–25, 1996.

Chong-Yung Chi (S'83–M'83–SM'89) was born in Taiwan, R.O.C., on August 7, 1952. He received the B.S. degree from the Tatung Institute of Technology, Taipei, Taiwan, in 1975, the M.S. degree from the National Taiwan University (NTU), Taipei, in 1977, and the Ph.D. degree from the University of Southern California, Los Angeles, in 1983, all in electrical engineering.

From July 1983 to September 1988, he was with the Jet Propulsion Laboratory, Pasadena, CA, where he worked on the design of various spaceborne radar remote sensing systems including radar scatterometers, synthtic aperture radars, altimeters, and rain mapping radars. From October 1988 to July 1989, he was a visiting specialist at the Department of Electrical Engineering, NTU. Since August 1989, he has been a Professor with the Department of Electrical Engineering, National Tsing Hua University, Hsinchu, Taiwan. He has published more than 90 technical papers in radar remote sensing, system identification and estimation theory, deconvolution and channel equalization, digital filter design, spectral estimation, and higher order statistics (HOS) based signal processing. He has been a reviewer for both *Signal Processing* and *Electronics Letters*. His research interests include signal processing for wireless communications, statistical signal processing, and digital signal processing and their applications.

Dr. Chi is an active member of Society of Exploration Geophysicists, a member of European Association for Signal Processing, and an active member of the Chinese Institute of Electrical Engineering. He is a technical committee member of both 1997 and 1999 IEEE Signal Processing Workshop on Higher Order Statistics (HOS) and the 2001 IEEE Workshop on Statistical Signal Processing (SSP). He is also a member of International Advisory Committee of TENCON 2001. He is a co-organizer and general co-chairman of 2001 IEEE Workshop on Signal Processing Advances in Wireless Communications (SPAWC-2001). Since 1983, he has served as a reviewer for several international journals and conferences, such as IEEE TRANSACTIONS ON SIGNAL PROCESSING, IEEE TRANSACTIONS ON CIRCUITS AND SYSTEMS, IEEE TRANSACTIONS ON GEOSCIENCE AND REMOTE SENSING, IEEE TRANSACTIONS ON COMMUNICATIONS. He was also conference session chair many times. Currently, he is an Associate Editor for the IEEE TRANSACTIONS ON SIGNAL PROCESSING.

Chii-Horng Chen was born in Taiwan, R.O.C., on December 2, 1970. He received the B.S. degree from the Department of Control Engineering, National Chiao Tung University, Hsinchu, Taiwan, in 1992. He is currently pursuing the Ph.D degree at National Tsing Hua University, Hsinchu.

His research interests include statistical signal processing, digital signal processing, and wireless communications.